

Review

Multi-Scale Surface Texturing in Tribology—Current Knowledge and Future Perspectives

Philipp G. Grützmacher ^{1,2}, Francisco J. Profito ³ and Andreas Rosenkranz ^{4,*}

¹ Institute for Engineering Design and Product Development, Tribology Research Group, TU Wien, 1040 Vienna, Austria; philipp.gruetzmacher@tuwien.ac.at

² Chair of Functional Materials, Department of Material Science and Engineering, Campus D33, 66123 Saarbrücken, Germany

³ Department of Mechanical Engineering, Polytechnic School of the University of São Paulo, São Paulo 17033360, Brazil; fprofito@usp.br

⁴ Department of Chemical Engineering, Biotechnology and Materials, University of Chile, Santiago 8370415, Chile

* Correspondence: arosenkranz@ing.uchile.cl; Tel.: +56-995-463-769

Received: 30 September 2019; Accepted: 25 October 2019; Published: 28 October 2019



Abstract: Surface texturing has been frequently used for tribological purposes in the last three decades due to its great potential to reduce friction and wear. Although biological systems advocate the use of hierarchical, multi-scale surface textures, most of the published experimental and numerical works have mainly addressed effects induced by single-scale surface textures. Therefore, it can be assumed that the potential of multi-scale surface texturing to further optimize friction and wear is underexplored. The aim of this review article is to shed some light on the current knowledge in the field of multi-scale surface textures applied to tribological systems from an experimental and numerical point of view. Initially, fabrication techniques with their respective advantages and disadvantages regarding the ability to create multi-scale surface textures are summarized. Afterwards, the existing state-of-the-art regarding experimental work performed to explore the potential, as well as the underlying effects of multi-scale textures under dry and lubricated conditions, is presented. Subsequently, numerical approaches to predict the behavior of multi-scale surface texturing under lubricated conditions are elucidated. Finally, the existing knowledge and hypotheses about the underlying driven mechanisms responsible for the improved tribological performance of multi-scale textures are summarized, and future trends in this research direction are emphasized.

Keywords: multi-scale surface texturing; hierarchical surfaces; numerical approaches; friction reduction; wear reduction

1. Introduction

As early as in ancient Egypt, tribology, which includes friction, wear, and lubrication, has been put to use to reduce frictional losses and mitigate interfacial damage between rubbing surfaces. During the construction of the pyramids, the Egyptians had already realized that the efforts involved in transporting heavy stones could be significantly reduced when putting rolling elements underneath the stones. Most probably, this can be considered as the first evidence that rolling friction is lower than pure sliding friction. Over the centuries, prominent researchers including Da Vinci, Newton, Amontons, Coulomb among many others have studied frictional phenomena under different aspects [1,2]. During their investigations, they realized that friction is governed by the interplay of various mechanochemical phenomena taking place simultaneously on the contact interface. To shed more light on the involved processes, they initially tried to describe the frictional behavior of dry sliding contacts from a phenomenological point of view by establishing a mathematical relationship between

the applied normal load and the resulting friction force. The definition of the coefficient of kinetic friction (COF) goes back to Amontons and Coulomb, who independently figured out that the resulting friction force is proportional to the normal load for dry sliding contacts [3]. The constant relating both forces is the kinetic COF. This simple, linear relationship often oversimplifies the complexities found in actual tribological interfaces, where time-dependent, non-equilibrium thermodynamic processes contribute to the resulting COF [4]. The Amontons-Coulomb's model of dry friction assumes that the kinetic COF does not depend on the nominal contact area and on the magnitude of the sliding velocity. These observations have been refined by Bowden and Tabor, who realized that the COF, in fact, does not depend on the nominal contact area but rather on the real contact area between the asperity peaks, thus connecting the resulting friction force with the real contact area and shear strength of the interface [5].

The real contact area strongly depends on the roughness of the interacting surfaces [6,7]. Since the surfaces are effectively in contact only at the tips of distinct asperities, all individual contact spots have to be summed up to determine the entire contact area. Having a closer look at the surface roughness, it becomes obvious that multiple scales are involved. Dependent on the respective instrument and magnification used to measure the surface topography, different geometric features become visible ranging from nanometer- to millimeter-scale [8]. This immediately demonstrates that the frictional properties of a contact pair depend on multi-physics phenomena occurring in multiple length scales, and therefore the accurate determination of the friction force relies on the solution of a multi-scale problem. Apart from the geometric and fractal aspects of surface roughness, mechanochemical effects on different scales also affect the resulting frictional behavior. Thinking about the atomic and molecular levels, the bonding strength directly correlates with the friction force. Furthermore, the atomic/molecular arrangement and order phenomena influence friction and wear. Considering order and crystal structures, chemical imperfections and lattice defects play a significant role in the subsequent materials and hence frictional properties. This impressively underlines that frictional behavior is also influenced by chemical contributions occurring on different scales. From an engineering point of view, friction and wear are also affected on micrometer- and millimeter-scale when tolerances of manufacturing processes are considered. This short paragraph ultimately demonstrates that tribology is highly inter-disciplinary and definitely encompasses the research and solution of multi-physics and multi-scale problems.

A detailed look into nature shows that it often makes use of multi-scale/hierarchical surfaces to optimize physical properties [8–11]. A well-studied phenomenon is the drag reduction observed for dolphins and sharks induced by their skin containing features of at least two different scales [12,13]. In addition, the ability to tune adhesion properties by hierarchical surface textures as observed for beetles, flies, geckos among others, is another prominent example of the important role of interfacial geometry [14–16]. Moreover, the lotus leaf, for instance, combines a specific surface roughness on different scales with modified surface chemistry to enable self-cleaning properties and superhydrophobicity [17,18].

Inspired by these strategies provided by nature and the direct impact of the surface topography on tribological performances, specific surface textures have been utilized for more than three decades to optimize friction and wear. The pioneering systematic work in this field has been carried out by Etsion and co-workers showing the potential benefits of surface textures in different lubricated machine components (seals and piston rings among others) [19,20]. Afterwards, this topic has experienced tremendous interest and attention in the tribological community. In the last years, several review papers have summarized the state-of-the-art regarding the influence of surface texturing on friction and wear in laboratory experiments and machine components [21–24]. Interestingly, the majority of the published research works make use of purely single-scale textures. The positive effects of single-scale textures depend to a large extent on the type of contact (conformal or nonconformal) and lubrication regime. Under full-film hydrodynamic lubrication, surface textures may function as micro-hydrodynamic bearings which boost the fluid pressure, thus increasing the overall load-carrying

capacity [25–28]. This is particularly significant for contacts with parallel and flat surfaces, such as those encountered in mechanical seals and parallel thrust bearings. Furthermore, the subambient pressure zones formed in textures close to the contact inlet due to the fluid cavitation phenomenon responsible for the aforementioned micro-hydrodynamic bearing effect may also contribute to drawing additional lubricant into the contact (inlet-suction effect) [27,29,30]. However, it needs to be pointed out that an inappropriate choice of texture parameters (i.e., texture depth, width, and density) may lead to detrimental effects due to the excessive increase of the cavitation zones, which may reduce the local film thickness and the load carrying capacity [31]. Under mixed lubrication, surface textures typically fulfill multiple functions. Besides contributing to improved hydrodynamic pressure they also reduce the real contact area and they are able to store lubricant thus acting as a secondary oil supply. Moreover, textures can trap wear particles thus reducing abrasive wear. Under boundary lubrication, surface texturing reduces the real area of contact and can induce the formation of pressure-induced boundary layers, thus lowering friction and wear [32,33]. The proper combination of the aforementioned aspects leads to a significant reduction of friction and wear, and/or to shift the transition between different lubrication regimes [34–36]. Considering dry friction, the reduction of the real contact area as well as the storage of wear particles can be named as the main effects contributing toward improved tribological properties [37–39].

Although nature provides numerous examples of the successful use of multi-scale textures for friction reduction, the transfer of these ideas to engineering applications has been scarcely realized. Therefore, it can be expected that multi-scale surface textures bear the tremendous potential to further optimize friction and wear properties in machine components. In this context, this review article aims at summarizing the existing articles in the field of multi-scale surface textures to improve friction and wear. First, potentially suited fabrication techniques will be reviewed, as well as discussing the advantages and shortcomings of these techniques. Afterwards, the article reviews the research conducted in biologically inspired multi-scale surface textures and their effect on friction and wear. The next section will summarize the numerical methods used to model multi-scale surfaces to predict potential friction and wear reductions. Finally, this article intends to outline the mechanisms responsible for the improved friction and wear behavior promoted by multi-scale textures as well as provide future research directions for improved texture designs.

2. Fabrication Strategies for Multi-Scale Surface Textures

Historically, numerous methods have been utilized to create surface textures for tribological applications. In this context, surface textures can be defined as geometric features following a deterministic pattern, which is intended to be engineered to induce certain surface functionalities [40]. Moreover, textures can have a preferential direction or be arranged in a random fashion [40]. The fabrication methods can be roughly divided into mechanical, chemical, physical, and thermal methods [41]. Examples for each group can be found in Table 1. A detailed overview of the individual families of surface texturing methods has been given in the form of tree structures by Costa and Hutchings [41]. The benefits and limitations of each texturing technique have to be considered regarding productivity, efficiency, geometric flexibility, accuracy, material flexibility, among others. The general geometry and accuracy of the produced textures significantly affect the tribological behavior of the generated surfaces [22,23]. In this regard, the pitch, depth, edge angle, and line accuracy of the texture features are all factors influencing the tribological performance [22]. Accuracy is especially important for multi-scale textures since textures have to be combined suitably and both patterns should be left intact during the texturing process. For patterned surfaces in general and particularly for multi-scale surfaces, the real area of contact and hence the resulting friction force is significantly influenced by the arrangement of the textural features [40]. Efficiency is a critical factor when thinking about large-scale production. This is especially true in case of patterning many components in industrial chains, which directly asks for a rather cheap and efficient texturing method [41]. Of a vast variety of texturing methods, laser texturing is the most advanced technique, which can be traced back to its high flexibility

in terms of materials and geometries, high speed, good accuracy, and excellent control over the textures' geometry [20,22,41–43]. Furthermore, laser texturing belongs to the methods which remove material from the surface and therefore creates more durable and shear resistant textures compared to other methods that add material to the surface (i.e., protrusions) [22].

Table 1. General classification and examples for each type of texturing method [41].

Type	Methods
Mechanical	Microcutting, Microcoining
Chemical	Chemical etching, chemical vapor deposition (CVD)
Physical	Physical vapor deposition (PVD), focused ion beam (FIB) texturing
Thermal	Laser interference texturing, electrical beam texturing

Having the generation of multi-scale surface textures in mind, they can be fabricated in a multi-step [44–49] or single-step [50–52] process. Naturally, single-step processes are less time-consuming, easier to integrate into production lines, and therefore more efficient. Moreover, multi-step processes, which consist of different steps but using the same equipment to produce textures on different scales, are more practical and efficient than combining two or more different texturing techniques to produce multi-scale surfaces. It has to be pronounced that every surface inherently shows texture features on several scales. During laser surface texturing, for example, ablated particles can be redeposited on the surface, creating a random nano-roughness [53]. However, this review shall be limited to such techniques, which deliberately engineer multi-scale surfaces.

In the literature, several review papers can be found summarizing methods to create surface textures for tribological applications [40–42]. Hence, here only techniques with a special connection to multi-scale surface texturing will be presented.

2.1. Multi-Step Processes

Generally speaking, almost every two texturing techniques can be combined to create multi-scale surface textures. Thereby, upon combining different texturing techniques, three factors have to be considered in particular: (i) the complexity of the individual processes and, hence, the overall effort for the texturing approach, (ii) the sequence of the texturing steps [54], and (iii) the respective size limitations of each method. Regarding tribologically effective surface textures, suitable texturing techniques are those which generate surface textures on significantly different scales. According to Hsu et al., wide and shallow textures improve the tribological behavior under hydrodynamic lubrication, whereas narrow and deep textures can reduce friction under mixed or boundary lubrication [55]. In their multi-scale approach, they used a triboindenter to fabricate the textures individually by nano-scratching. As shown in Figure 1, they manufactured a polished reference sample, single-scale textures, a mixture of different dimples as well as different overlapping dimples. Such mechanical texturing methods for which a specific pattern can be programmed and then machined (CNC machining) offer the advantage of very flexible texture arrangements. Nevertheless, such processes are rather slow, since every texture feature has to be created individually, which results in strong limitations regarding their industrial applicability [22].

Similarly, laser surface texturing can be used to create multi-scale textures by ablating predefined surface areas, whereby each feature is created individually. Therefore, the laser beam is directed to the desired surface areas either by moving the sample via a translation stage or by scanning the beam over the sample surface with a galvanometric scanner [42,56–58]. In between the spots where the textures are to be created, the laser beam can be blocked by a shutter system. The general texture shape and their morphology can be influenced by the laser parameters like laser fluence, wavelength, and pulse duration as well as the focusing system [59–63]. The technique for which the laser beam is merely focused and scanned over the sample surface is called direct laser writing (DLW). Using laser surface texturing and specifically DLW, Segu et al. created multi-scale textures on steel samples for tribological

purposes [64–66]. Examples of these textures are depicted in Figure 2. In this regard, it needs to be highlighted that again the advantage of this technique is the flexibility in terms of geometrical shapes, but it lacks speed, especially when creating very small texture features.

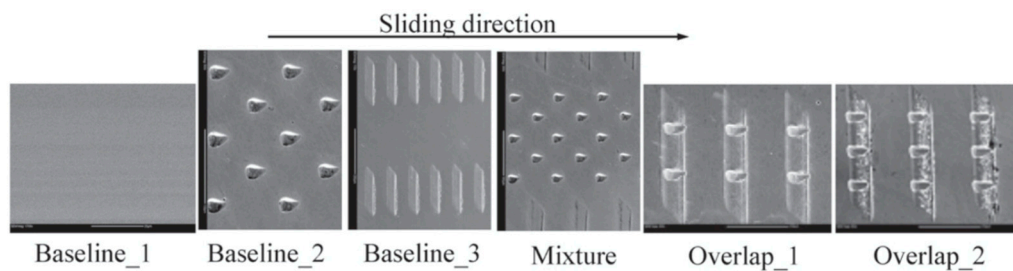


Figure 1. Multi-scale surface textures fabricated by nano-scratching using a triboindenter. In this work, single-scale, mixed, and overlapping textures have been produced. Adapted from [55].

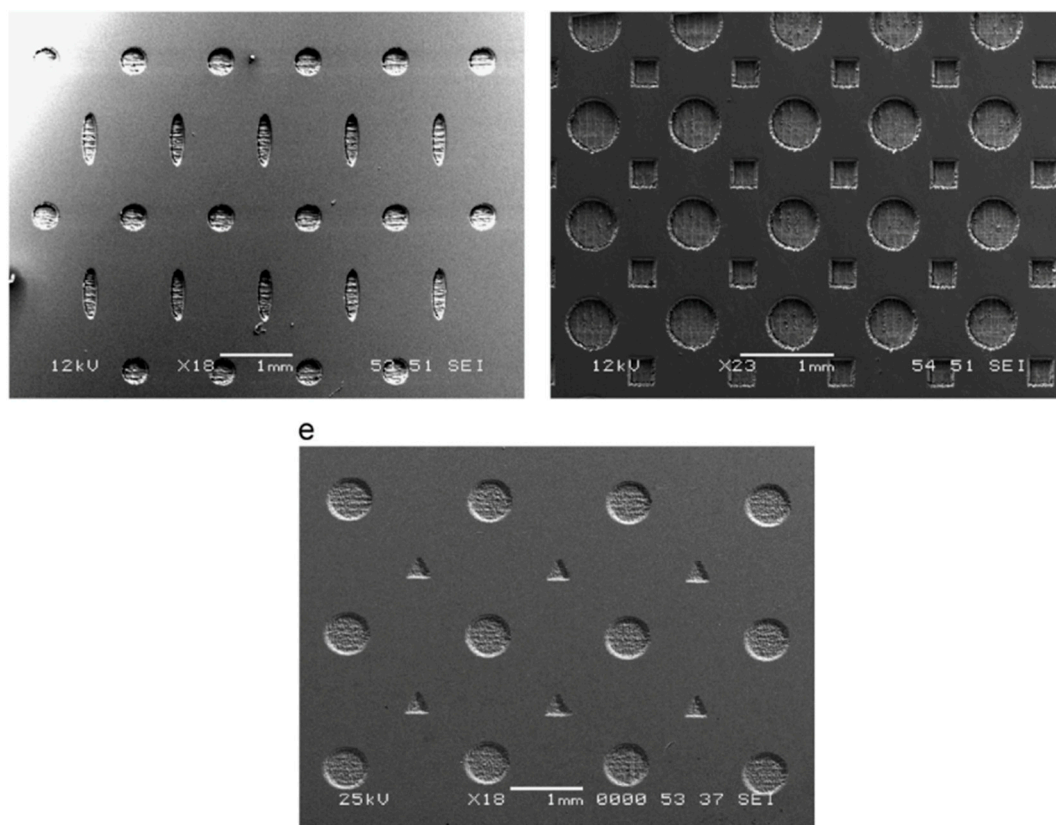


Figure 2. Multi-scale surface textures created by laser surface texturing using a pulsed Q-switched Nd:YAG laser with a power of 24 W and a pulse duration of 200 ns. The smaller textures (squares, triangles) have a side length of 250 μm while the bigger circles have a diameter of 500 μm . Adapted from [66].

Additionally, chemical methods like etching processes can be used to create multi-scale textures [67,68]. Wang et al. used a combination of lithography and reactive ion etching to create multi-scale textures consisting of bigger circular dimples with a diameter of 350 μm and smaller square dimples having a side length of 40 μm on silicon carbide to improve its tribological properties. The advantage of these chemical methods is that the surface topography is modified while the chemical and mechanical properties of the surface remain fairly constant [42]. Furthermore, material removal can be efficiently controlled, the design of the surface textures is flexible, and irregular shapes and complex geometries can be textured. However, the method is constituted by rather complex procedures

like lithographic methods and deep textures are rather difficult to obtain due to electrolyte diffusion and ohmic polarization. Moreover, it is expensive to create high-resolution textures, and less versatile regarding possible materials than laser surface texturing [22,42].

Furthermore, different texturing methods can be combined to create multi-scale textures [47–49,54,69–74]. Resendiz et al. used end milling with a single crystal diamond cutter and micro shot-blasting to produce multi-scale surface textures on aluminum [47]. The bigger circular dimples fabricated by machining had a diameter of 150 μm and a depth of 30 μm . The smaller textures created by shot blasting with 10 μm aluminum oxide particles are completely covering the underlying primary machined textures and can be found inside the dimples and on the non-textured portions between the dimples. Their depth is not given but the roughness increases by 88% to 0.33 μm compared to the flat surface. With a similar method using laser surface texturing and micro shot-blasting with 25 μm alumina particles, Kim et al. manufactured multi-scale surfaces on sapphire wafers [73]. Thereby, the micro-patterns created by the laser process had a depth of 100–300 μm and a diameter of 40–160 μm . In contrast, the shot blasted textures are with a surface roughness (R_q) of 450 nm much smaller, even though their exact dimensions are not given. Gachot et al. and later Grützmaier et al. combined micro-coining with laser surface texturing, specifically direct laser interference patterning (DLIP), to create multi-scale surfaces [48,49,54,70,72]. DLIP is a technique, which uses overlapping laser beams to modulate the laser intensity spatially by interference. By applying this technique, multiple texture features can be created on the surface in a single laser shot [62]. Micro-coining is a fast process, which allows for the generation of high-quality textures in the range of 20–200 μm at low cost, while DLIP is a fast and versatile technique especially suited to create smaller textures with feature sizes between 200 nm and 30 μm [54]. It is shown that the process sequence is important for this combination. Thereby, micro-coining should precede the laser process because the inverted process sequence may lead to the partial destruction of the laser textures especially in highly deformed areas, such as the flanks of the micro-coined textures [54]. If performed correctly, however, this approach can lead to pronounced multi-scale textures with a homogenous distribution of both texture types over the surface, as can be seen in Figure 3.

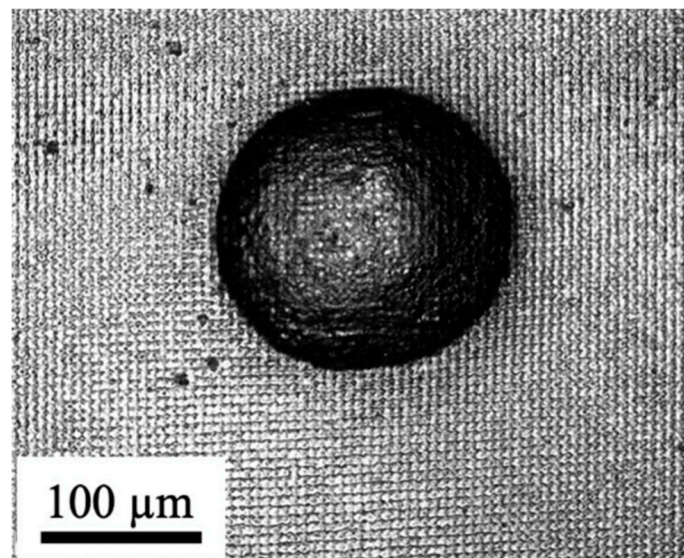


Figure 3. Multi-scale surface textures created by a combination of micro-coining and direct laser interference patterning. The bigger micro-coined textures have a diameter of 180 μm and a depth of 43 μm , whereas the cross-like laser pattern has a width of 6 μm and a depth of 0.6 μm . Adapted from [70].

Additionally, multi-scale textures can be manufactured by replicating natural surfaces inhibiting a multi-scale surface topography like the lotus leaf [44–46,75]. Shafiei and Alpas mimicked the natural

surface texture of lotus leaf and boa's skin using a cellulose acetate film. In a subsequent step, a nanocrystalline nickel layer is deposited onto this film to obtain the positive surface texture of the natural sample [45,46]. To add surface textures on another scale to the lotus leaf replicas, an additional electrodeposition step was used, which led to the deposition of spherical nickel droplets on the tips of the micro-textures as shown in Figure 4 [46].

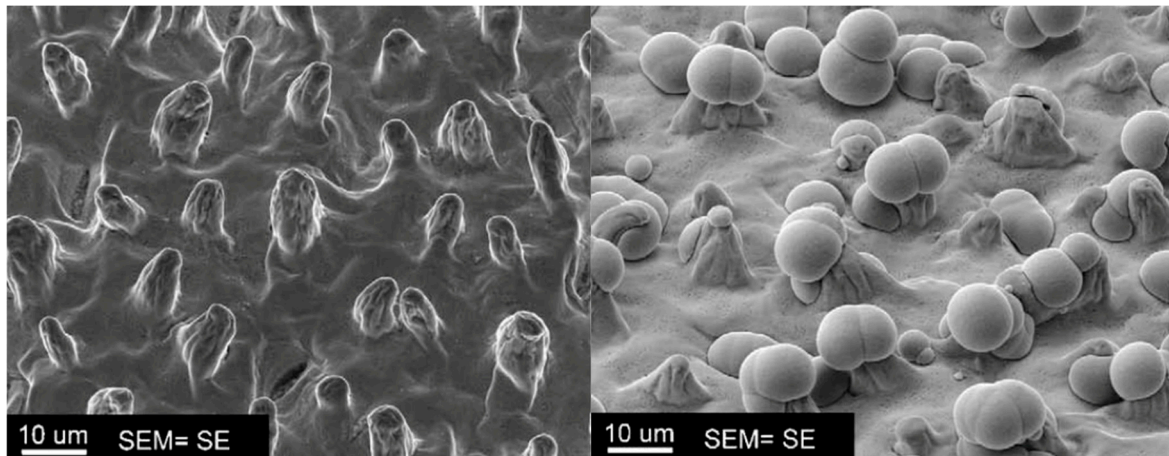


Figure 4. Multi-scale surface textures on nickel created by replicating the natural surface of the lotus leaf and a subsequent electrodeposition step. Adapted from [46].

Finally, an innovative method to create multi-scale surface textures is to combine two different laser processes, namely DLW and DLIP [76,77]. Thereby, the bigger surface textures are created by DLW and the smaller textures by DLIP. This eliminates the disadvantage of low productivity for DLW when creating small textures and offers the advantage of creating both texture types with the same tool even though a two-step fabrication process is used. Thinking about the industrial application of such textures, this means that only one tool needs to be integrated into the production process leading to smaller costs and higher production speeds. Cardoso et al. used this technique to create multi-scale surface textures. They used a solid state laser having a pulse duration of 30 ns for the DLW process fabricating cross-like textures having a periodicity (distance from channel to channel) of 15–35 μm , a depth of 3–5 μm and a width of 15 μm . Subsequently, the smaller textures were fabricated with a DLIP system on top of the bigger DLW textures using an Nd:YVO₄ laser with a pulse duration of 10 ps. The smaller textures showed a periodicity of 2.6 μm and a depth of roughly 1 μm [76]. Another laser process, which has been proposed to create multi-scale textures is the combination of DLW with the controlled generation of laser induced periodic surface structures (LIPSSs) [78]. Zhang et al. used this approach to fabricate multi-scale textures. The primary textures fabricated by DLW have a width of 40 μm and a depth of 50 μm , whereas the LIPSSs on top of these textures have a depth of merely 150 nm and a period of 550 nm [78].

It is worth mentioning that several other techniques like self-assembly of nanostructures by thermal evaporation [17,79], nano-imprinting [80] or special etching techniques [67] can be utilized. However, these techniques are quite complicated and not well suited for industrial applications.

2.2. Single-Step Processes

Single-step processes to create multi-scale patterns are scarcely spread. However, some can be found in the literature [59,81–83]. However, often these multi-scale patterns occur rather randomly. Qiu et al. used an electrochemical growth approach to fabricate multi-scale cobalt textures [82]. In their work, they demonstrated cobalt crystals with several levels of hierarchy having a flower-like morphology.

However, a single-step method to fabricate multi-scale samples in a controlled fashion is again the laser process. By making use of the formation of LIPSSs during laser processing with suitable laser parameters, bigger laser textures can be created by DLW, while simultaneously smaller LIPSSs are formed [81]. Ahmmed and Kietzig used a femtosecond Ti:sapphire laser system with a wavelength of 800 nm and a pulse duration <85 fs to fabricate multi-scale textures on copper [81]. The laser inscribed primary pattern demonstrated a width of 14–80 μm and a depth of 60–130 μm whereas the LIPSSs were on a scale of several hundred nanometers. Thereby, the primary textures can be controlled by the laser parameters (i.e., laser power, pulse duration, scanning speed, etc.), whereas the secondary LIPSSs textures can be controlled by the laser wavelength, the incidence angle, and the polarization of the laser beam [57].

3. Effect of Multi-Scale Textures on Friction and Wear—Experimental Studies

A significant amount of research work has been conducted to replicate the multi-scale surface topographies of the Lotus leaf, the Rice leaf, shark skin, snakeskin, among others and test these surface with regard to their potential to optimize friction and wear under dry and lubricated conditions. Shafiei and Alpas fabricated bio-inspired multi-scale surface textures by mimicking biological surfaces such as the Lotus leaf and the snakeskin using replica film followed by the electrodeposition nanocrystalline nickel. For the replicated, multi-scale Lotus leaf sample, a 30% reduction of the maximum COF under dry sliding was observed compared to a flat surface. The authors attributed the observed effect to a reduction of the real contact area [45]. Following the same approach, Shafiei and Alpas fabricated multi-scale surfaces by replicating the Lotus leaf and combining it with a chemical surface treatment (PFPE) to achieve superhydrophobicity and low friction. Using this combined treatment, a maximum friction reduction of 60% under dry friction was shown, which was explained by the reduction of the real area of contact [46]. Similarly, Wang et al. fabricated bio-inspired superhydrophobic surface textures in nickel (Lotus- and Rice-leaf) by combining a replicating technique with nickel electroplating. Though this approach, multi-scale surface textures with protruding and depressing textures were realized. The final fabrication step was a chemical modification of the resulting surface textures, applying PFPE as a lubricant. Afterwards, they studied the tribological behavior of the fabricated surface textures with and without final PFPE surface treatment. The best performance with significantly reduced COFs over the entire sliding time was found for the multi-scale surface textures with subsequent PFPE treatment irrespective of the type of textures (protruding or depressing). Additionally, they verified that the wear resistance was improved when using a final chemical PFPE treatment. The observed results were traced back to the good lubrication abilities of PFPE films as well as the possibility to reduce the real area of contact and to trap wear particles in the surface textures [44]. Using a combination of nanocasting, electroplating, and physical vapor deposition, Wang et al. fabricated diamond-like carbon films with Lotus leaf-like textures thus aiming at generating hard and flexible coatings with superhydrophobicity and good tribological properties. The main drawback of this innovative idea is the number of steps necessary to fabricate these surfaces. The fabricated textures showed a pronounced reduction in the COF over time with PFPE lubrication (without any further oil), which was traced back to the possibility to store wear particles [84]. However, it remains questionable if this is really the only contributing aspect leading to the improved friction and wear performance. The research group of El Mansori has put considerable attention to the analysis and imitation of python skin [43,85,86]. In their tribological investigations under dry conditions, they impressively demonstrated that pythons naturally have tribologically optimized surface features, which would be worth to mimic by laser surface texturing. The main conclusion of these works is that reptile skin typically follows an aperiodic and asymmetric pattern, which is in contrast to the deterministic idea of surface texturing such as arranging dimples or other shapes in a regular matrix. It can be figured that by copying more ideas from nature, improved texture designs with superior friction and wear performance can be achieved [43,87]. The research group led by Greiner conducted research towards a similar direction thus copying the surface texture of snakes and lizards to optimize

the friction response under dry and lubricated conditions. They verified that these bio-inspired surface textures reduce the COF by about 40% under dry conditions, while a 3-fold friction reduction was observed in lubricated systems [88,89]. Moreover, Greiner et al. observed a pronounced size effect when fabricating and testing multi-scale surface textures with variable diameter. Surface textures with the biggest diameter showed the lowest frictional results. The explanation of the obtained results is not straight-forward and requests more in-depth analysis of the underlying phenomena, which will be subject of ongoing research work [89].

Wang et al. studied the tribological performance of textured SiC contacts under water lubrication. Initially, they verified a 2.5-fold increase in the critical load (for the transition from full-film to mixed lubrication) for single-scale textures with the lowest area density, a low depth, and an intermediate diameter [90]. In a follow-up paper, they used reactive ion etching to fabricate multi-scale textures having small and large dimples to optimize the texture effect of SiC–SiC pairings by increasing both the hydrodynamic pressure (big dimples) and the lubricant supply (small dimples). The multi-scale texture showed the best tribological performance under water lubrication with a 3.3-fold increase in the resulting load carrying capacity (Figure 5). The authors attributed the positive effects induced by surface textures to an additional hydrodynamic pressure and lubricant reservoir effect. Additionally, surface textures helped to improve the running-in process, thus leading to a smoother surface with lower roughness values. In the case of the multi-scale surface, it was speculated that the finer textures improved the water supply, thus offering more water in the tribological contact zone, which is beneficial to induce tribochemical reactions between water and SiC [91]. A summary of the research conducted by Wang et al. on textured SiC surfaces can be found in [92].

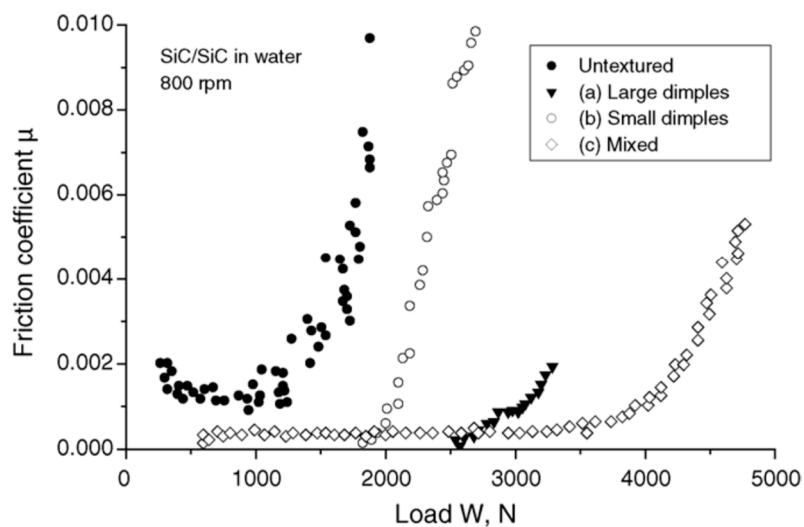


Figure 5. Coefficient of kinetic friction (COF) versus load curves in order to determine the critical load for an untextured reference as well as single-scale (large and small dimples) and multi-scale surface textures (mixed). Adapted from [91].

Segu et al. studied the effect of multi-shape textures combining circular, elliptical and triangular textures using a pin-on-disk set-up. The texture combination was fabricated by laser surface texturing using a nanosecond ND-YAG laser with a pulse duration of 200 ns. For all combinations, the structural depth was kept constant at 6.5 microns. Moreover, two area densities, namely 12 and 20%, were selected. The authors recorded Stribeck-like curves and compared the frictional behavior of the multi-shape surfaces with two reference surfaces (grinded and polished). All texture combinations showed beneficial frictional properties with a faster transition (i.e., at lower sliding speed) to low frictional values indicating hydrodynamic lubrication. In addition, they also proved the possibility to positively affect the friction and wear performance under dry sliding conditions using multi-shape textures. The textures showed a reduced averaged COF, which was traced back to the possibility to store

wear debris in the textures thus removing it from the tribological contact. Furthermore, they also demonstrated beneficial frictional properties under lubricated conditions for longer sliding times. The beneficial effects of these multi-shape surfaces under lubricated conditions were explained by the increased possibility to build-up additional hydrodynamic pressure [66]. The contribution presented by Segu et al. gives interesting insights into the frictional behavior of multi-shape surfaces under dry and lubricated conditions but lacks on the presentation of carefully selected reference measurements. The data of the grinded and polished references are not sufficient to really justify the frictional efficiency of the multi-shape surfaces since the tribological results of single-shape textures (purely circular, elliptical, and triangular) have not been presented for comparison. Following the promising results of the combination of circular and elliptical multi-shape textures, Segu et al. fabricated multi-shape textures consisting of circular and elliptical textures having a depth between 3.5 and 7.5 microns as well as a density between 5 and 20%. With regard to the structural depth, they verified the best frictional behavior with the lowest COF for an intermediate depth of 5.5 microns. They explained this observation with the interplay between the oil film thickness, the structural depth of the textures and the potential pressure build-up. Although demonstrating interesting results, this study again lacks the presentation of suitable reference data as well as a deep elucidation of the obtained results [65].

The research group of Hsu conducted also important research related to the effects and mechanisms of surface textures in tribological contacts. An initial study aimed at investigating different texture geometries under low load and high-speed conditions as well as under high load and low speed conditions. Related to the first conditions, elliptical textures oriented perpendicular to the sliding direction led to the best results with the greatest friction reduction under boundary and mixed lubrication. Different contributions such as reserve lubricant flow, cavitation, the storage of lubricant inside the textures as well as a squeeze effect must be taken into consideration and may act simultaneously. Under high load and low speed conditions, all surface textures induced detrimental effects with increased friction, which has been mainly traced back to undesired edge effects [93]. Following this systematic study on single-scale surface textures with the main conclusions that large/shallow textures reduce friction under full-film lubrication and small/deep textures are effective under mixed and boundary lubrication, Hsu et al. extended their texture design to multi-scale surface textures. The general idea was to combine small but deep textures with large but shallow textures to be efficient under different lubricated conditions. Hence, Hsu et al. created a mixture of textures on different scales but also followed design rules found in nature, which favor an overlapping of textures on different scales, as shown in Figure 1 in Section 2. For experiments performed under a low contact pressure, all textured samples irrespective of single- or multi-scale were efficient to reduce friction. Particularly, the multi-scale textures with overlapping features showed a maximum friction reduction of up to 80% (Figure 6). Even under higher contact pressure, this multi-scale texture reduced friction by 70%, which is a significant advance in the design of surface textures for high contact pressure applications. Moreover, the multi-scale samples showed negligible wear features, which was traced to the transition from mixed to full-film lubrication even under higher contact pressures. Generally speaking, this study impressively demonstrated that by combining surface textures on different scales (each one optimized for a different lubrication regime) can bring an overall improvement of the frictional performance with a significant friction reduction across all lubrication regimes [55].

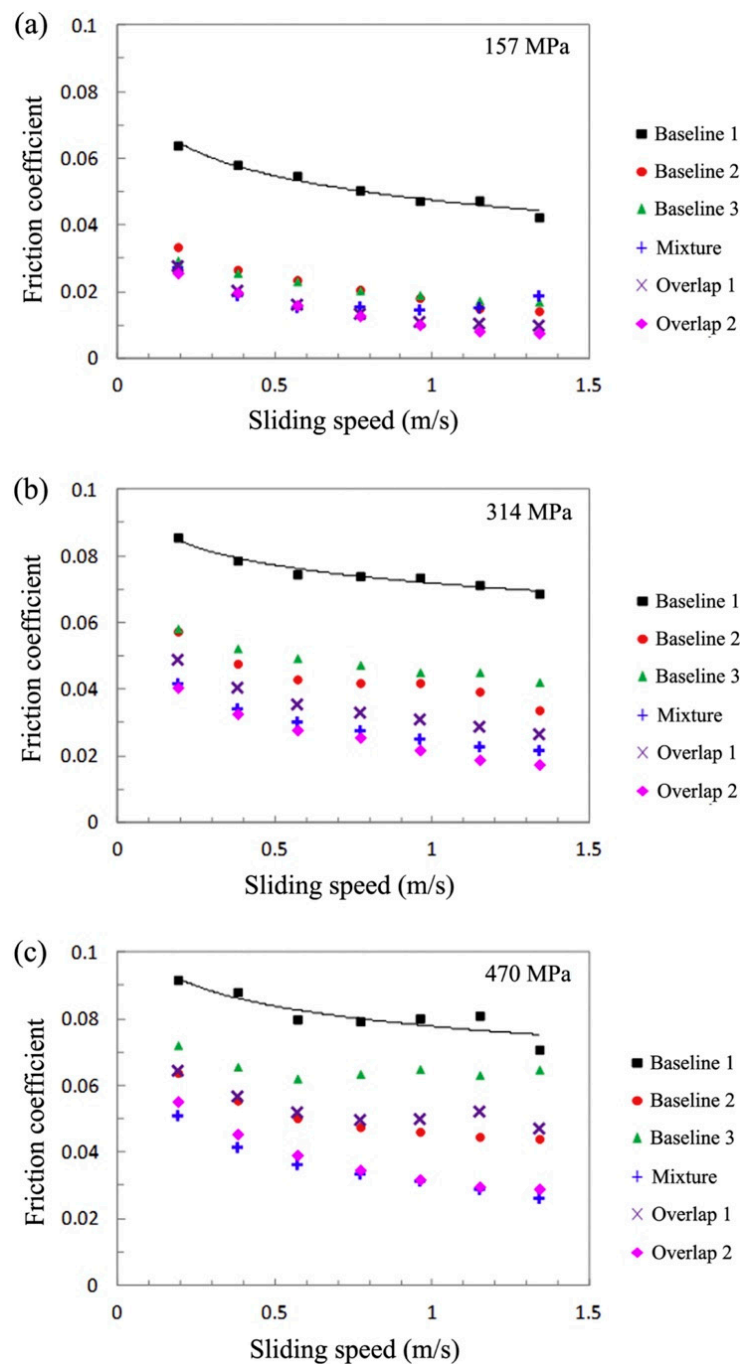


Figure 6. COF versus sliding speed for different reference cases (polished and single-scale textures) and different designs for multi-scale surface textures (mixture and overlapping textures) depending on the acting contact pressure (a) 157 MPa, (b) 314 MPa and (c) 470 MPa. The black baseline represents the polished reference surface, whereas baseline 2 and 3 stand for the single-scale surface textures. Adapted from [55].

Inspired by a significant friction reduction induced by micro-coined dimples as verified by [94], Grützmaier et al. overlapped micro-coined surfaces with finer textures fabricated by direct laser interference patterning (DLIP). For their study, they selected hemispherical micro-coined surfaces having a depth of 50 and 95 microns. Single-scale micro-coined samples with a depth of 50 microns showed beneficial frictional results, while deeper micro-coined samples demonstrated detrimental results regarding friction and wear. With this selection of the micro-coined geometries, Grützmaier et al.

aimed at addressing the effect of additional finer cross-like laser textures thus answering the question whether this kind of texture pattern may improve the frictional behavior of single-scale samples and either compensate the negative effects of deep dimples or further improve beneficial samples. Interestingly, the overlapped laser textures downgraded the frictional behavior of the initially beneficial micro-coined sample with a depth of 50 microns. In contrast, the additional laser textures helped to significantly improve the frictional behavior of the sample with a depth of 95 microns. Another interesting aspect has been realized during the analysis of the resulting wear scars. For both multi-scale samples, the wear scars show a rather irregular behavior with deflections from its original, circular trajectory. For this to happen, the tribological counter-body (ball) needs to interact with the underlying surface textures, which reflects the potential pressure build-up induced by the textures. Grützmacher et al. interpreted the obtained results in the following way. The improved friction behavior of the multi-scale texture was traced back to potentially reduced cavitation. For deep structures, it is well known that cavitation is more likely to occur. Combining deeper, coarser textures with fine cross-like textures may, therefore, help to reduce cavitation thus improving the distribution of lubricant in the contact area. This may induce a larger oil film thickness, thus increasing the resulting load-bearing capacity and reducing friction [48]. Following this approach, Grützmacher et al. investigated the effect of single- and multi-scale surface textures applied on the shaft of journal bearings by recording Stribeck-like curves. In order to manufacture these textures, DLIP and roller-coining have been utilized. Though DLIP, finer cross-like textures with a periodicity of 6 microns and a depth of about 1 micron have been realized, while roller-coining aimed at fabricating coarser textures with depths of up to 45 microns. Compared to the polished reference shaft, all textured single- and multi-scale surfaces led to a significant improvement of the frictional performance. As can be seen in Figure 7, under mixed lubrication, a reduction of friction by a factor of about 2–3 was observed, whereas, under hydrodynamic lubrication, a 4.6 fold decrease of the resulting COF was observed for the multi-scale texture combining the finer cross-like laser textures with the deeper micro-coined textures. The improved friction behavior of the aforementioned multi-scale texture was traced back to potentially reduced cavitation. Combining deeper, coarser textures with fine cross-like textures may help to reduce cavitation thus increasing the load bearing capacity as well as reducing the COF under hydrodynamic lubrication [72]. A comprehensive overview of the research efforts of Grützmacher et al. related to the effect of multi-scale surface textures in tribological contacts can be found in [71].

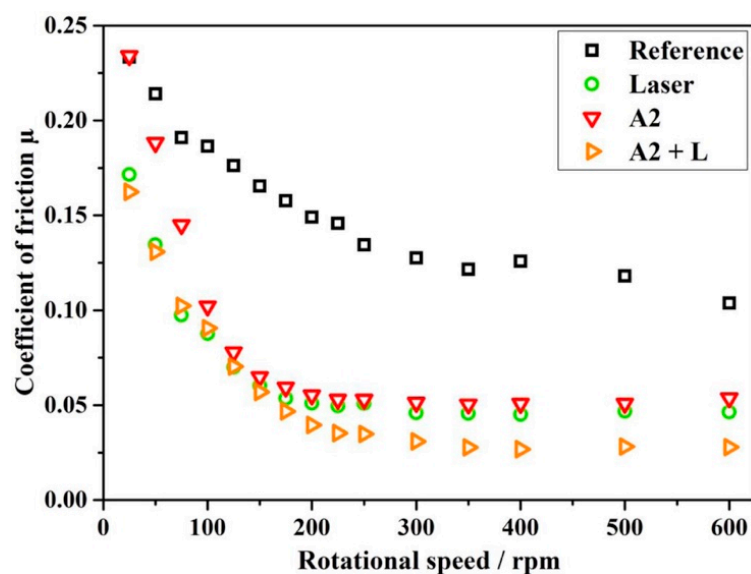


Figure 7. COF versus rotational speed for an unpolished reference, a purely laser-textured sample (laser), a solely micro-coined sample (A2) and the respective multi-scale samples combining direct laser interference patterning (DLIP) and micro-coining. Adapted from [72].

Inspired by the positive effects of multi-scale textures related to the running-in behavior and the transition between mixed and full-film hydrodynamic lubrication, Rosenkranz et al. studied the friction and wear performance of these textures under mixed lubrication. Following the beneficial effects observed for single-scale textures fabricated by DLIP [34] and micro-coining [94], they combined cross-like DLIP textures (depth about 0.6 microns and periodicity about 6 microns) with hemispherical micro-coined textures inhibiting two different depths and periodicities. Using an additive-free PAO oil, Rosenkranz et al. investigated the temporal evolution of the COF over time with a special emphasis on the time when the COF suddenly increases, which has been defined as the maximum oil film lifetime. The largest effect in terms of extending the oil film lifetime has been found for the sample with the deepest and widest micro-coined textures combined with the cross-like laser texture (Figure 8). The obtained results were attributed to an improvement of the lubricant's distribution and the additional pressure build-up due to the finer laser texture, while the coarser micro-coined texture tended to store produced wear particles thus removing them from the tribological contact zone [70].

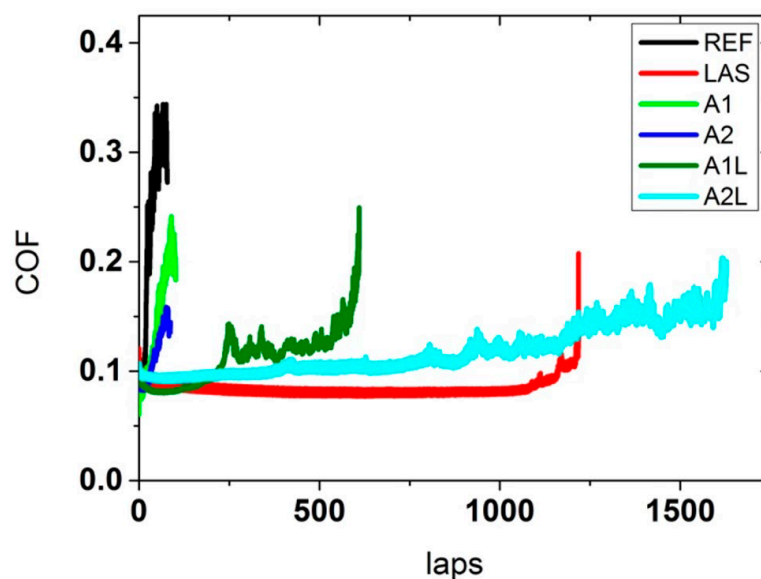


Figure 8. COF versus laps in order to determine the maximum oil film lifetime of the polished reference, the cross-like laser textures (LAS), the micro-coined surfaces (A series) and both corresponding multi-scale textures (A1L and A2L). Adapted from [70].

As already outlined in Section 2, Resendiz et al. have combined inclined end milling and micro shot blasting to create multi-scale surface textures in aluminum samples. Using end milling, circular-shaped dimples with a diameter of about 75 microns and a depth of 30 microns were created, while shot blasting with aluminum oxide particles (diameter of 10 microns) superimposed a finer roughness of the coarser milled textures. Using experimental and numerical approaches, the authors tried to evaluate the respective effect of each texturing method as well as the combination of both under lubricated conditions. In Stribeck-like curves, surface textures fabricated by the combination of end milling and shot blasting showed the best frictional behavior with a significant friction reduction compared to the untreated reference surface (Figure 9). The observed experimental findings were addressed by simulations thus verifying a cavitation effect inducing an additional pressure build-up around the textured surfaces. For the textures fabricated by a combination of both techniques, the greatest film thickness was found. Additionally, they proved that the tribological performance was notably improved by the storage of wear debris, which underlines that two effects are responsible for the superior friction and wear behavior of the multi-scale surface textures [47].

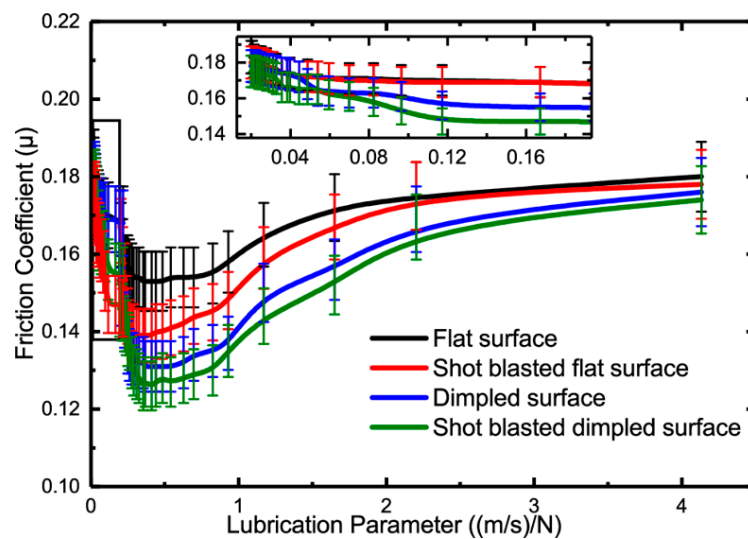


Figure 9. COF versus lubrication parameter for a flat surface, a shot-blasted sample, a dimpled sample, and a shot-blasted dimpled (i.e., multi-scale) surface. Adapted from [47].

Zhang et al. used pulsed nano-second and femto-second lasers to fabricate micro- and nano-scale surface textures as well as a combination of both ending up in a multi-scale texture. After having fabricated the respective textures, all surfaces were covered by a TiAlN coating. While the general idea is promising, the tribological characterization of the fabricated samples is not sufficient to draw any significant conclusion. Additionally, the combination of texturing and coatings is further complicated by the use of MoS₂ as a solid lubricant. As already outlined in Section 2, the combination of lasers having a different pulse duration is promising in the context of creating multi-scale textures, but simpler tribological experiments need to be conducted in order to explore the full potential of this approach [78].

4. Effect of Multi-Scale Textures on Friction and Wear—Numerical Approaches

The design of optimum surface textures devised to improve the tribological performance of contacting interfaces can be considerably improved by using numerical simulation tools. Using numerical approaches to simulate the frictional behavior of multi-scale textures, the interplay of several physical factors (i.e., thermal effects, complex rheology, asperity contacts, surface wettability and the intricate lubricant flow as well as percolation) acting simultaneously on different lengths scales in the tribological contact zone can be investigated to facilitate the design of effective multi-scale textures. Complementary, numerical results can be useful to shed light on the underlying mechanisms responsible for the observed friction and wear reduction (e.g., micro-hydrodynamic bearing, inlet-suction, oil reservoir, and debris trapping effects), the improved sealing performance (e.g., lubricant channeling and percolation effects) and the finer contact temperature control induced by multi-scale textures. Therefore, optimum texture parameters (e.g., texture shape, size, depth, density) could be determined for specific applications and working conditions.

In this regard, three main modeling approaches, namely (i) computational fluid dynamics (CFD), (ii) Reynolds-type equation formulations based upon deterministic and averaging/homogenization methods, and (iii) numerical multi-scale techniques, are frequently used to simulate the tribological behavior of textured surfaces in different lubrication regimes. It is important to notice that not all modeling approaches presented in the following sections have already been applied specifically to the simulation of multi-scale textures. Nevertheless, most of the discussed methods and techniques can be extended to accomplish advanced analysis concerning the lubrication performance of contact interfaces with multi-scale textures. Thus, this review also intends to pave the way for future developments of more sophisticated approaches to model multi-scale surface textures.

4.1. CFD Modeling

The first modeling approach makes use of CFD simulations based upon the full solution of the Navier–Stokes (N–S) equations. The main advantage of CFD is the possibility of considering advanced mathematical models and complex flow phenomena, such as inertia and thermal effects, turbulence, cavitation, fluid compressibility and rheology, wall slip, fluid-structure interaction, among others. The major drawback of CFD simulations resides in the huge, and often prohibitive, computational efforts necessary to simulate problems involving textured surfaces due to the inherent fine meshes needed to properly discretize local geometric features. Particularly considering multi-scale textures, several works investigated the influence of hierarchical structures of bio-inspired shark-skin surfaces on friction drag reduction under turbulent conditions. Choi et al. explored the behavior of the turbulent micro flow field on bio-inspired micro-grooved surfaces using direct numerical simulation (DNS) [95,96]. The distribution of the micro flow field over the real shark-skin surface and its effect on the drag reduction were also analyzed through CFD simulations by Zhang et al. [97] and Luo et al. [98,99]. Figure 10 shows the morphology of scales of shark-skin surfaces studied by Luo et al. [98,99], including a schematic diagram illustrating one of the factors responsible for the drag reduction (Figure 10c) and numerical results obtained from CFD simulations (Figure 10d). The authors concluded that the drag-reduction mechanism of shark-skin is a combination of four factors: (i) a decrease of the wall viscous friction due to reduced turbulence next to the walls induced by the micro-groove tips, which stick out the viscous sub-layer, (ii) a decrease of the turbulence intensity near the wall due to the back-flowing phenomenon associated with the micro-droplets with opposite direction to the main flow (see Figure 10c), (iii) a super-hydrophobic effect produced by the boundary slipping phenomenon on the fluid-solid interface, which significantly decreases the velocity gradient and the local viscous resistance on the surface, and (iv) the presence of a nano-chain of mucus covering the wall, which increases the thickness of the viscous sublayer thus producing the aforementioned slipping phenomenon.

More recently, Martin and Bhushan conducted large-scale CFD simulations to optimize shark-inspired riblet geometries and dimensions for low drags. In that work, it was highlighted that the underlying mechanism responsible for the drag reduction was also associated with vortices lifted away from the surface and hence formed over the riblets (see Figure 11a) under turbulent flow conditions thus decreasing the overall shear stress. Furthermore, it has been identified that the optimum size of riblet design features for low-drag and anti-fouling surfaces can range from nano- to micro-scale depending on the size of the physical components for specific applications [100]. A numerical and experimental investigation of different marine drag reduction technologies based upon shark-skin inspired riblet surfaces was carried out by Fu et al. Illustrative examples of CFD analyses conducted by the authors for herringbone riblets are shown in Figure 11b. They demonstrated that triangular-shaped riblets presented a better trade-off between manufacturing and drag reduction [101].

CFD simulations were also applied by Belhadjamor et al. to study the effect of texturing on the anti-fingerprint and self-cleaning performance. It was verified that multi-scale textures are capable to decrease the finger contact area and promote hydrophobicity thus reducing the surface affinity to skin oil [102]. An example of finite element simulation and contact angle and wettability analysis of a hierarchical textured surface for anti-fingerprint and self-cleaning applications is illustrated in Figure 12. Regarding tribological applications, Brajdic-Mitidieri et al. used a CFD model with cavitation to analyze the lubricant flow behavior, load support and friction of linear, convergent pad bearings having a closed pocket. Depending on the bearing's convergence ratio and the pocket's location, the authors identified two different mechanisms responsible for friction reduction: (i) at moderate to high convergence ratios, the reduction of the shear stress is more pronounced than the pressure build-up within the pocket when the textures are suitably positioned in the high pressure region of the bearing, thus reducing the COF, and (ii) at low convergence ratios, the boost in hydrodynamic pressure within the pocket due to its convergent geometry generates higher load support (and lower friction) compared to the non-textured case [103]. A CFD-based thermo-hydrodynamic study was

carried out by Vakilian et al. to explore the characteristics of Rayleigh step bearings under different steady conditions [104].

Many other works have been published in the literature involving the use of CFD analysis with different model complexities to investigate the lubrication performance of single scale textured thrust and journal bearings. The reader is referred to [21] for a thorough review of recent works based on CFD analysis to investigate the lubrication performance of single scale textured bearings. Furthermore, despite the studies of [103,104] were not directly associated with multi-scale textures, the methodologies adopted can be used as a reference for more advanced CFD analysis involving multi-scale textures.

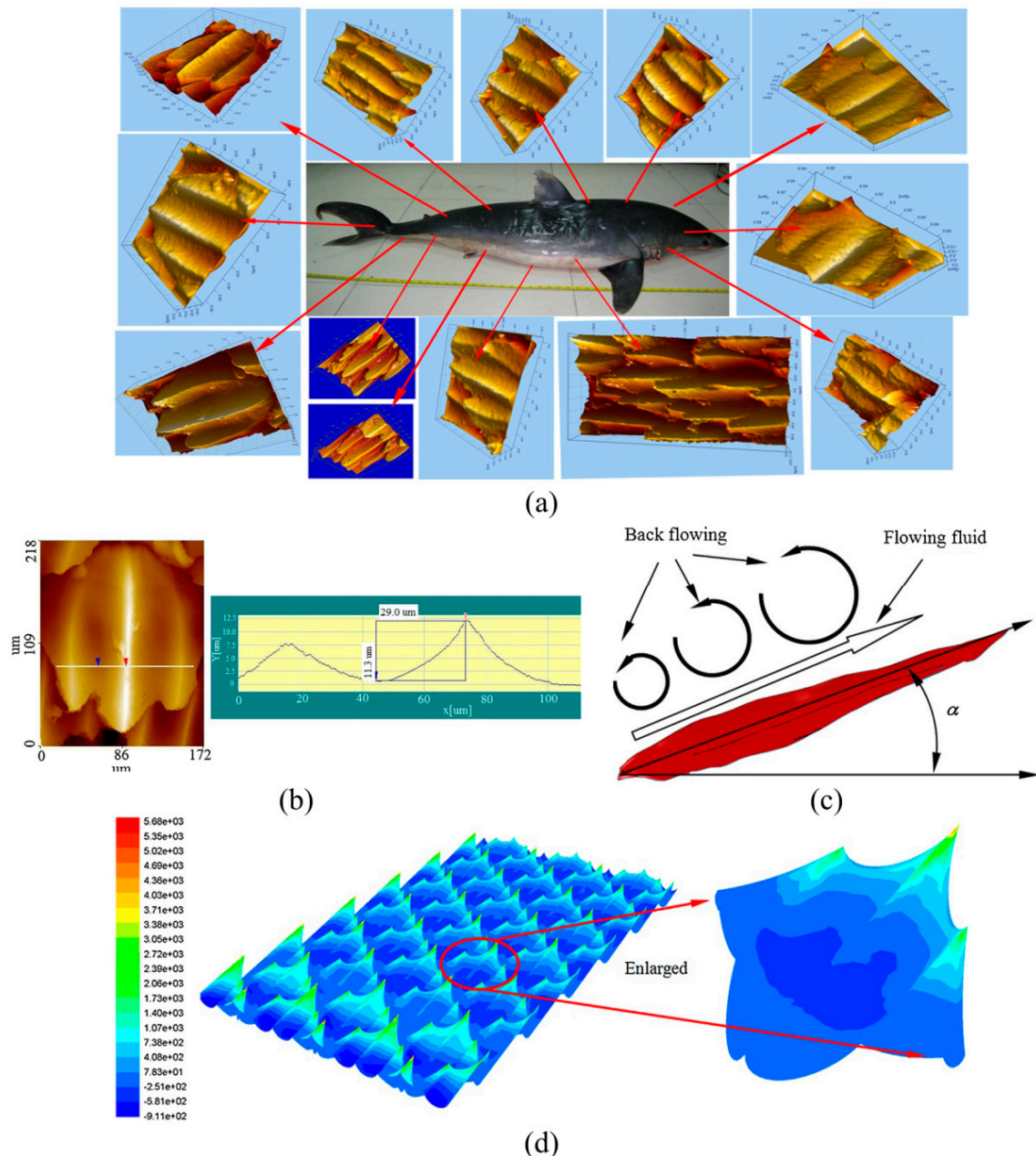


Figure 10. Hierarchical structures of bio-inspired shark-skin surfaces for friction drag reduction. (a) Morphology of scales on different locations of the sharkskin. (b) 3D image of a biological single shark-skin scale and the corresponding cross-section profile. (c) Schematic diagram of the back-flowing phenomenon responsible for the drag reduction due to the attenuation of the turbulence intensity. (d) Computational fluid dynamics (CFD) simulation of the resulting shear stress over a real shark-skin surface as well as detailed distribution over a single scale surface. Adapted from [99].

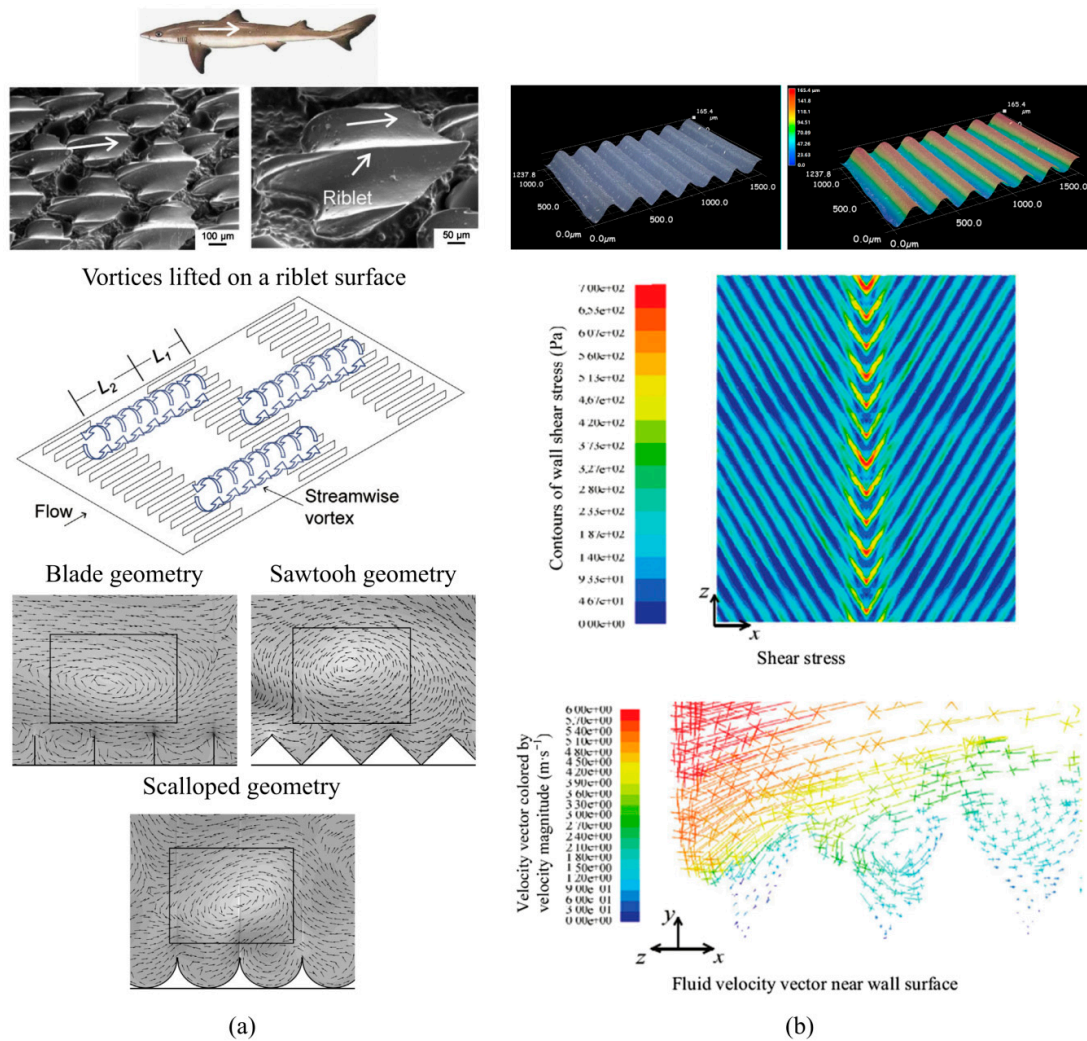


Figure 11. Shark-inspired riblet geometries for low drag applications. (a) Top: micrographs of samples acquired by scanning electron microscopy. Middle: schematic of the streamwise vortices lifted mechanism responsible for drag reduction on riblet surfaces. Bottom: velocity fields obtained by CFD simulations showing the vortices lifted on blade, sawtooth and scalloped riblet geometries. (b) Top: 3D surface topography measurement of micro-riblets applied to marine drag reduction technologies. Shear stress distribution (middle) and velocity field (bottom) of herringbone riblets obtained by CFD simulations. Adapted from [100,101].

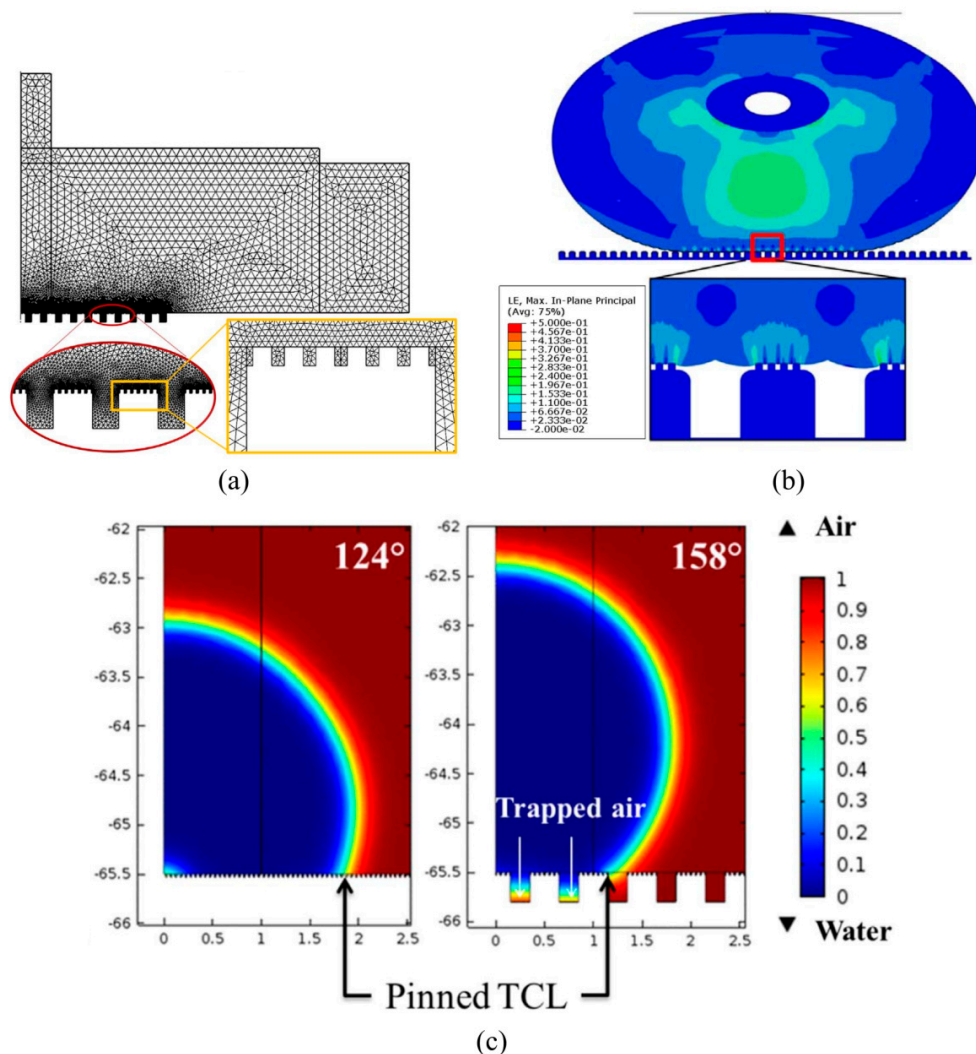


Figure 12. Hierarchical textured surface for anti-fingerprint and self-cleaning applications. (a) Finite element mesh. (b) Deformed shape and strain distribution. (c) Contact angle and wetting state for hydrophobicity analysis. Adapted from [102].

4.2. Reynolds-Type Equation Modeling

The second modeling approach is based upon the solution of the Reynolds equation derived from the thin fluid film lubrication theory. The advantage of this approach is the lower computational cost required to simulate textured contacts compared to full CFD methods. Furthermore, many modified versions of the Reynolds equation exist, in which specific physical aspects such as thermal effects, cavitation, turbulence, lubricant rheology, as well as the influence of surface roughness on the lubricant flow (important for mixed lubrication analysis) have been incorporated. Particularly, some methods commonly used to account for the influence of surface roughness on lubrication can be extended to predict the lubrication performance of multi-scale surface textures. In this sense, a brief explanation of the most important models used for mixed lubrication analysis shall be presented here. Special emphasis has been put on works in which such models have been applied to investigate the lubrication behavior of multi-scale surface textures. In this regard, two classes of methods based upon the Reynolds equation approach, namely deterministic and multi-scale, need to be distinguished. Each class is defined according to the way the components of the surface topography are considered for the mathematical representation of the fluid film gap geometry.

4.2.1. Full Deterministic Methods

In deterministic methods, full-scale representation of the surface topography, including both micro- and macro-scale features of the surface texture, alongside roughness, are considered in the definition of the lubricant film thickness and solution of the Reynolds equation. In the last few decades, quickly advancing computational power and the development of improved numerical techniques (e.g., multi-grid methods and parallel computing) permitted the effective digitalization of engineering surfaces, as well as the efficient solution of the coupled contact mechanics and lubrication problems. Therefore, increasing attention has been devoted to deterministic simulations. Early deterministic solutions of full-film EHL under limited rough contact were proposed for artificial topographies with simple irregularities, such as dimples and sinusoidal waviness [105–109]. Actual 2D roughness profiles were then employed by [110,111] and later 3D measured topographies were considered by [112,113]. More recently, Hu and Zhu [114–125] proposed a fully coupled mixed-TEHL model assuming a continuous lubricant film in the non-contacting regions as well as asperity contact wherever the local fluid film is sufficiently thin. In this model, the film thickness is computed from the deformed average gap, while the lubricant flow and asperity interactions are accounted for in a unified solution framework. Using this formulation, different types of multi-scale surface textures can be used as input data to deterministically simulate the entire transitions from full-film and mixed-TEHL as well as boundary lubrication under more severe conditions. However, since no averaging technique is considered in this formulation, it can only be applied to relatively small regions such as point contacts. The Hu and Zhu deterministic model was applied by [121,126] to propose a virtual surface texturing simulation tool being able to provide comparative information and directions for innovative texture design and optimization, including the relationship between textured surfaces and mixed lubrication characteristics of non-conformal contacts. Figure 13 illustrates examples of different groove textures evaluated with the deterministic mixed-TEHL model proposed by Hu and Zhu. The full-scale mixed-TEHL model developed by Hu and Zhu was also coupled to different multi-scale surface texture decomposition models to investigate the influence of surface roughness [127] and groove texture patterns placed on cylinder surfaces of internal combustion engines [128,129] on the COF.

Li and Chen proposed a deterministic mixed-lubrication model applied to the simulation of the piston ring cylinder liner contact of internal combustion engines. The model is based upon the calculation of the oil transport and the hydrodynamic pressure generation for the contact between a parallel and flat rigid plane sliding against a rough surface [131–135]. Similarly, Profito et al. presented a deterministic mixed-lubrication model based upon the simultaneous solution of the asperity contact and fluid flow problems at the roughness scale considering inter-asperity mass-conservative cavitation. The influence of the cylinder liner wear on the lubrication performance of a Twin Land Oil Control Ring (TLOC) was analyzed using measured surface topographies of a honed cylinder liner prior to and after 100 h engine tests (see Figure 14a). The results showed that under mixed lubrication, the worn liner surface yielded to an increase of the average hydrodynamic load capacity and a decrease of the asperity contact pressures compared to the unworn liner surface. As illustrated in Figure 14b,c, this was traced back to the smoothing of the plateau regions caused by the wear-out of the highest asperities and the general decrease in the summits curvature, which contributed to facilitate the pressure-driven lubricant flow throughout the inter-grooves zones thus intensifying the role of the honing grooves in the hydrodynamic pressure generation [130]. Afterwards, Tomanik et al. applied the deterministic mixed-lubrication model proposed by Profito et al. to investigate the effect of waviness and roughness of two measured mirror-like coated bore topographies on the hydrodynamic and asperity pressure distributions. The simulation results revealed that most of the fluid pressure was generated by the honing grooves rather than by the localized pores on the coated bore surfaces [136]. Moreover, Biboulet et al. and Noutary et al. proposed multi-grid techniques to solve deterministic hydrodynamic lubrication models with non-mass-conservative cavitation for the piston ring cylinder liner contact with measured textured surfaces. It was shown that the groove depth and density are

important factors determining the load carrying capacity, whereas the groove shape has only a minor influence [137–139].

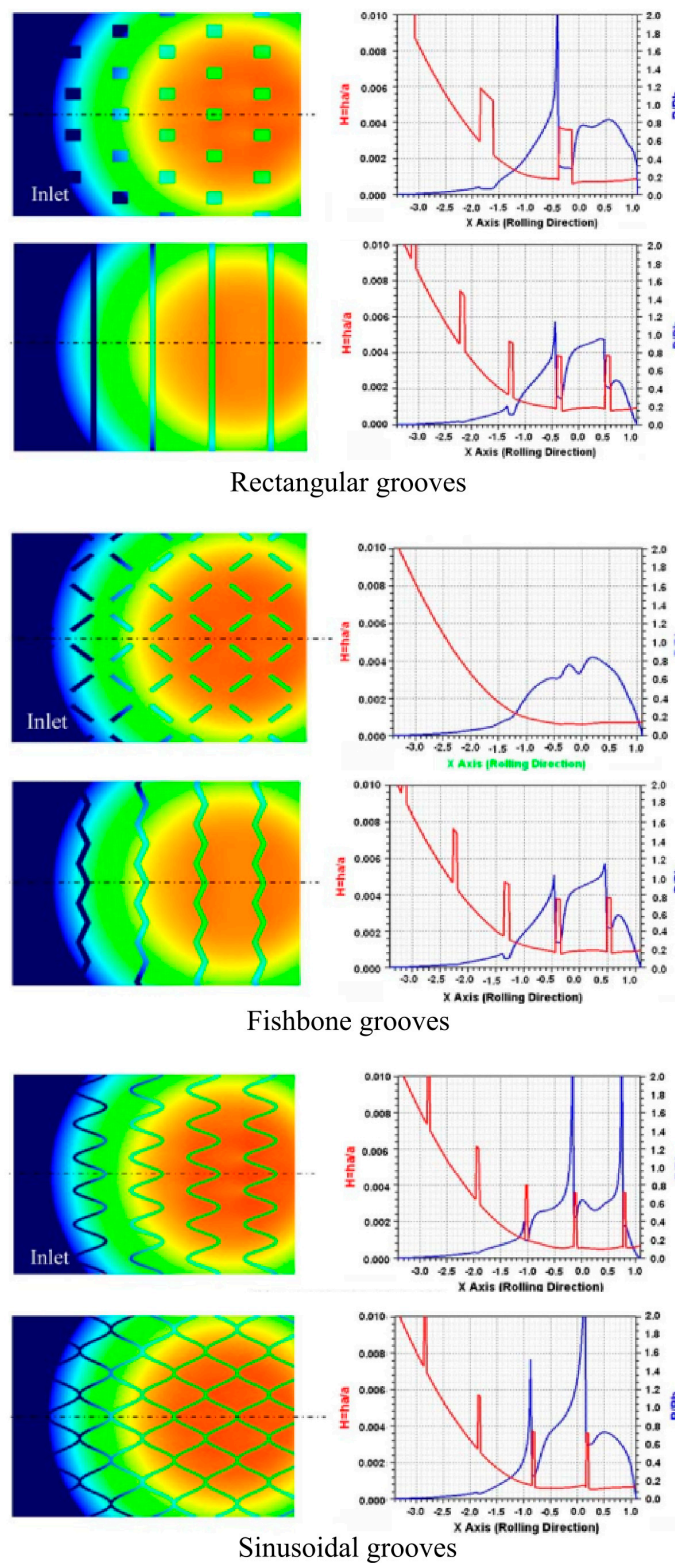
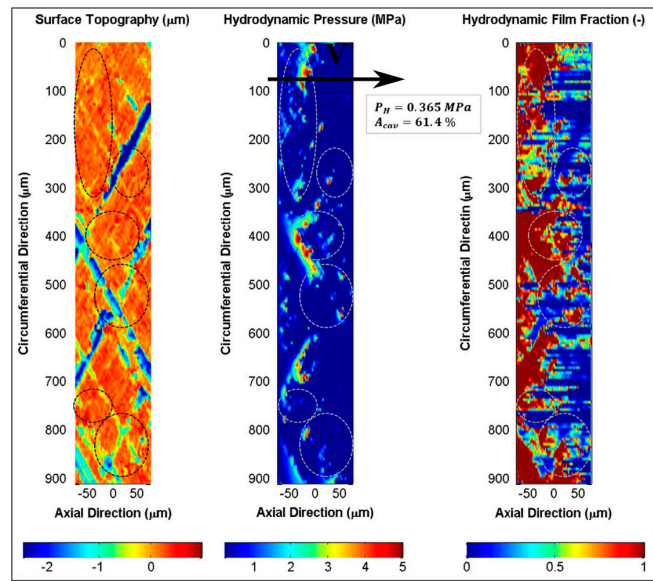
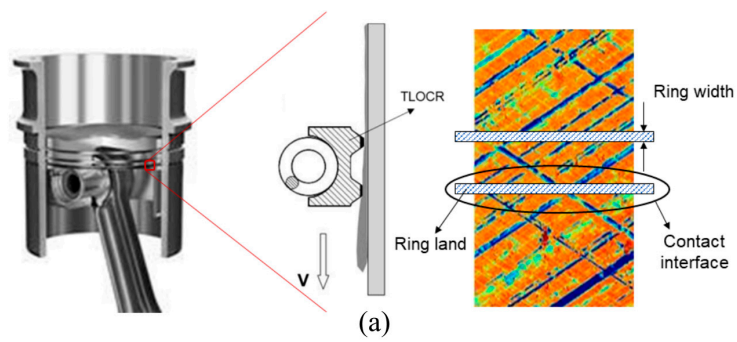
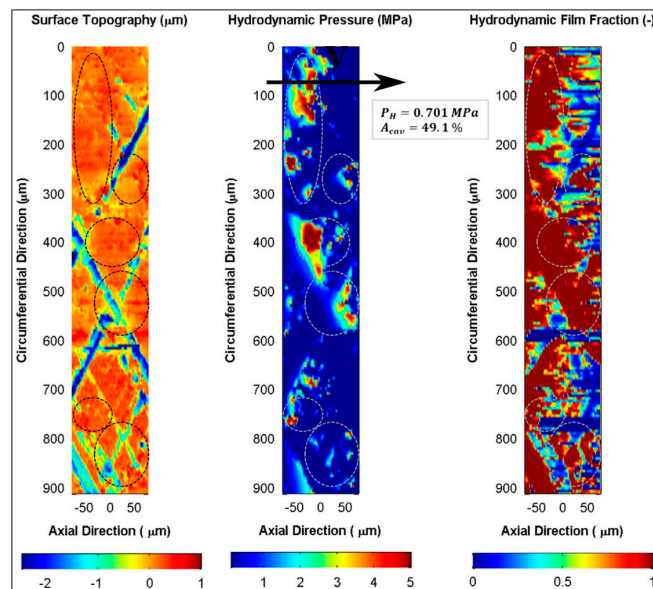


Figure 13. Deterministic simulations obtained with the fully coupled mixed-TEHL model proposed by Hu and Zhu. Sample cases with textured surfaces: rectangular (left), fishbone (middle) and sinusoidal (right) grooves with corresponding film thickness counters, centerline pressures, and normalized film thicknesses. Adapted from [118].



(b)



(c)

Figure 14. Influence of cylinder liner wear on the lubrication performance of a Twin Land Oil Control Ring (TLOCR) investigated by deterministic simulations. (a) Schematic of the TLOCR system and cylinder liner topography. (b) Field results for an instantaneous position of the TLOCR land on the liner prior to the engine test. (c) Field results for the same instantaneous position of the TLOCR land on the liner after 100 h engine test. Dashed circles highlight regions with most significant changes after wear. Adapted from [130].

A deterministic mixed lubrication model was also proposed by Minet et al. for mechanical seals applications. The model is based on the simultaneous solution of the Reynolds equation with mass-conservative cavitation and asperity contact considered through the Hertzian contact model. The results reproduced numerically the hydrodynamic load carrying capacity between nominally parallel surfaces promoted by the surface roughness, as well as the transition from mixed to full hydrodynamic lubrication regimes in face seals [140].

4.2.2. Analytical Multi-Scale Methods

Despite the better accuracy of fully deterministic methods, the computational efforts required in these cases are often prohibitive in practical applications due to the fine meshes needed to properly capture the local features. This is especially true for multi-scale surface textures, for which very fine meshes would be necessary to discretize the lubrication domain to entirely represent the geometric details of all scales. Therefore, different analytical multi-scale methods, especially averaging and homogenization methods, have been proposed to avoid dense discretization grids. In these methods, the overall influence of the surface texture features, along with the roughness in mixed lubrication analysis, are represented in terms of averaging parameters (flow factors and homogenization factors) introduced in the governing equations (e.g., averaged Reynolds equation) defined over the entire macro-scale lubrication domain. Thus, only the overall macroscopic geometry of the contacting surfaces is effectively considered in this analysis. The overall calculation process of the flow factors used in the averaged Reynolds equation is schematically illustrated in Figure 15. It is important to emphasize that most of the analytical multi-scale methods discussed in the following paragraphs have been initially proposed to model solely the effect of roughness on lubrication. Nevertheless, they can be extended to deal with the different length scales of multi-scale textures. For a deeper understanding of the principles and fundamentals of multi-scale modeling in science and engineering, the interested reader is referred to the comprehensive textbooks [141–144]. Particularly with respect to tribology, the reader is referred to [145] for an extensive review on modeling and simulation of various physical, chemical and mechanical phenomena across different scales.

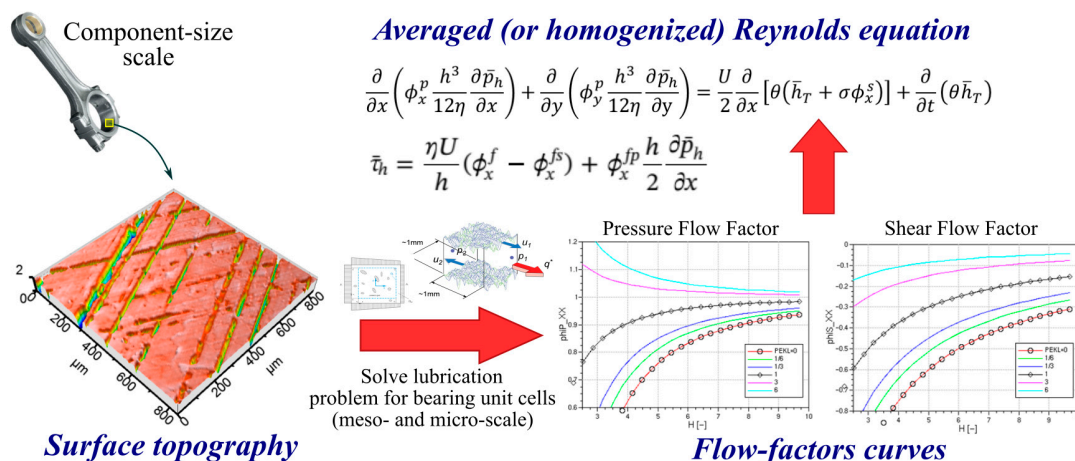


Figure 15. Schematic illustrating the calculation process of the flow factors (or homogenization factors) used in the averaged (or homogenized) Reynolds equation which, underlay most analytical multi-scale methods. The flow factors can be calculated either from measured surfaces of actual engineering components or from virtually generated topographies. The flow-factor curve on the left shows the variation of the pressure flow-factor as a function of the dimensionless average interfacial separation. The pressure flow-factor has significant impact on the calculation of the hydrodynamic pressure under mixed lubrication conditions. Similarly, the flow-factor curve on the right represents the variation of the shear flow-factor, which influences the shear stress (and thus friction force) calculations.

Averaging Flow Methods

The modeling of the effect of surface roughness patterns on lubrication was first reported by Tzeng and Saibel [146] for one-dimensional transversal roughness and followed by Christensen [147–149] and Chow and Cheng [150] for two-dimensional transverse and longitudinal topographies. All of these pioneering works have been established within the framework of the stochastic process theory, which is based upon the concept of viewing the film thickness as a stochastic process that results in a Reynolds-type equation for the mean or expected fluid pressure.

Patir and Cheng [151,152] proposed an average flow model for general roughness patterns by incorporating “flow factors” coefficients directly in a modified Reynolds equation that is solved in the smooth global domain. The flow factors are determined independently by solving the local deterministic flow problem for a specified rough surface. Unlike the Christensen’s methodology that particularly weights the film thickness oscillations according to an expectancy operator defined for a given roughness height distribution, the Patir and Cheng model is derived by “locally averaging the lubricant flows at the microscopic scale” for a representative rough bearing cell. This provides specific flow factors coefficients allowing for the consideration of the roughness (or other length scale components) induced flow perturbation effects directly on the global lubricated domain. The major drawback of this approach is a consequence of its heuristic derivation, which poses limitations on dealing with eventual crossflow produced in the case of surface roughness anisotropy. Such lack of generality was first highlighted by Elrod [153] and subsequently by different authors, including Tripp [154], who proposed a more complete tensor form of the averaged Reynolds equation. In the latter, the effects of roughness anisotropy on lubrication are accounted for in the off-diagonal terms of the diffusion and convective flow tensors, in particular, when the off-diagonal terms are negligible, the Tripp model is essentially identical to the model proposed by Patir and Cheng.

The Patir and Cheng average flow model has proven to be effective to predict the mixed lubrication performance for a wide range of applications, such as thrust and journal bearings, piston and piston-ring cylinder bore systems, mechanical seals, rolling element bearings, gears, and cam-tappet contacts, etc. Regardless of the tribological application, an important aspect for the efficacious use of any average flow model refers to the proper calculation of the flow factor coefficients for a specified topography. Furthermore, the consideration of rough contact mechanics and micro-cavitation effects also significantly affect the accuracy of the flow factor coefficients. In many successful cases, deterministic simulations of representative bearing unit cells at different length scales have been carried out to estimate the flow factors, as reported in several publications involving surface textures [155,156], honing grooves [157,158] and general roughness patterns [159–162].

A comparison between a deterministic hydrodynamic model and the stochastic solution based upon Patir and Cheng approach was undertaken by Dobrica et al. [163] for a partial journal bearing operating under mixed-EHL. The results underlined that the stochastic model correctly predicted the tendencies produced by the different roughness patterns in the fluid pressure distribution and average minimum film thickness, but underestimated the friction torques on both shaft and pad.

A multi-scale method based on the averaging flow concept was proposed by de Kraker et al. [155,156] for surface textures under mixed lubrication including micro-cavitation. In their approach, the local (micro) flow effects for a single micro-scale texture unit cell were evaluated through CFD simulations, and the results were then averaged to flow factors to be used with an averaged Reynolds equation on the macro-scale bearing level. The flow factors are dependent on the ratio between film thickness and texture dimensions, surface velocities and pressure gradient over a texture cell. Additionally, the method presented has no restrictions to the texture dimensions and shape, so that it could be well extended to model multi-scale surface textures.

Homogenization Methods

The modeling of the fluid flow problem in mixed lubrication has been addressed by Bayada [164–168], Jai and Bou-Saïd [169–171] and Buscaglia [172–174] within the framework of the

homogenization theory for spatially periodic roughness. This approach is based upon the derivation of a homogenized Reynolds equation, defined at the macroscopic global scale, which captures the overall effects of the surface roughness on the lubricant flow. Besides posing the average flow model on a more rigorous mathematical base that overcomes the pure heuristic induction of the Patir and Cheng model, one additional feature of these techniques is the proper definition of the local (or auxiliary) problem, which has to be solved over a periodic unit cell to compute the average flow tensors [175]. Thus, similarly to the average flow models, the effects occurring at different length scales are incorporated in the homogenized (averaged) Reynolds equation from the solution of well-posed local problems.

A series of works have been published by Almqvist which contributed to the consolidation and widespread use of homogenization methods in lubrication applications [176–181]. The homogenization method proposed by Almqvist has been used to investigate the effect of roughness and surface texture on the tribological performance of different machine elements, such as piston-ring cylinder liner contact and rotating devices [179,182–187].

More recently, Rom and Muller [188] proposed a reduced basis method to accurately solve and speed-up the solution of the homogenized Reynolds equation in a finite element framework. This method replaces the computationally expensive solution of the full texture cell problems (micro-scale) with a reduced basis problem of much smaller dimension, which provides a significantly accelerated solution strategy. After the solution of the texture cell problem for a range of film thicknesses, the homogenized finite element matrix and vector are computed to assemble the homogenized problem. The effectiveness of the combined use of both the homogenization method and reduced basis technique is evaluated for textured journal bearings.

A novel homogenized approach was proposed by Scaraggi et al. [189,190] to study the mixed lubrication behavior of steady sliding contacts of elastically soft solids. The coupled effects of asperity-asperity and asperity-fluid interactions have been considered through a mean field theory based upon a perturbation treatment. The results demonstrated how the asperity flattening induced by the fluid-asperity interactions, as well as the local percolation effects and roughness anisotropic deformation govern the fluid flow at the interface. It was also remarked that the lubrication regime is generally not uniform at the interface due to different local average separations. Furthermore, the potential occurrence of an apparent (elasto)-hydrodynamic regime for those lubrication conditions characterized by values of $\bar{h}/h_{rms} \leq 1$ at the macroscopic level was discussed, for which the lubricant is expected to have a negligible influence on the frictional stresses. This effective transition from boundary to (elasto)-hydrodynamic regime for a given value of \bar{h}/h_{rms} occurs due to the increase of the defined sliding parameter $U\eta/(E^*h_{rms})$, which determines a transition from a constant boundary stress value to a power-law shear stress. It was further noticed that this transition disappears for very small values of \bar{h}/h_{rms} , when percolation takes place and the average fluid flow vanishes. Afterwards, Scaraggi [191–193] also presented a homogenized method based upon the application of the Bruggeman effective medium to the Reynolds equation to investigate the average effect of textured surfaces on the macroscopic hydrodynamic characteristics of the interface. The method allows for the assessment of generic texture shape, distribution and area density, and was applied to practical cases involving 1D and 2D thrust bearing geometries.

A heterogeneous multi-scale method has been proposed by Gao and Hewson [194] to analyze micro-EHL with small-scale topographical features. The small-scale problem was solved using full CFD simulations including local elastic deformations and coupled to the global scale via scattered data interpolation method. It has been demonstrated that the proposed multi-scale framework successfully modeled the global pressure and film thickness for a textured bearing while maintaining the small-scale modeling features. Later on, Gao et al. [195] extended this multi-scale framework by incorporating the micro-cavitation and local fluid shear thinning properties.

The homogenized Reynolds equation, which simultaneously considers surface roughness and turbulent flow effects, was proposed by Lahmar et al. [196]. A plain journal bearing with

periodic isotropic roughness patterns operating under turbulent conditions was used as a case study. The homogenized results agreed well with results obtained from deterministic simulations, showing that the proposed homogenization approach is suitable to study problems with rough surfaces and turbulent conditions.

A promising computational engineering framework was developed by Waseem et al. [197,198] to support the design process of optimized surface textures for hydrodynamic lubrication. The proposed framework makes use of a combination of a two-scale homogenization method and topology optimization schemes. Another important aspect of the developed multi-scale framework is the consideration of the temporal (squeeze-film effect) and spatial (wedge effect) variations in film thickness in the constitutive tensors, which characterize the homogenized response of the surface texture in terms of fluid pressure generation and load carrying capacity on the macroscopic scale. Although temporal and spatial variations in the film thickness are important for the generation of hydrodynamic pressure within the fluid at the interface, they are not always simultaneously considered in homogenization methods applied to lubrication problems.

More recently, Yildiran et al. [199] investigated the lubrication response of conventional textures (i.e., textures with well-defined, smooth geometries, such as dimples, squares, ellipsoids, V-shapes, etc.) and representative modern re-entrant textures (i.e., textures with more complex geometries, such as trapezoidal and T-shaped features) based upon the homogenization scheme proposed by Bayada and Chambat [164]. After a comprehensive review of the literature on homogenization techniques applied to lubricated contacts and their limitations, the transition between three microscopic lubrication regimes has been demonstrated for conventional and re-entrant textures. In this work, the difference between Reynolds and Stokes roughness is also discussed. In all the above-mentioned references, except [199], the local roughness slope is always assumed small (Reynolds roughness), so that the flow equations at the microscopic scale are well described by the Reynolds equation (i.e., the local inertia effects can be neglected without significant loss of accuracy). When larger local roughness slope is present (Stokes roughness), the local inertia effects need to be taken into account in the analysis, for instance, through the solution of Stokes equations.

4.2.3. Semi-Deterministic Methods

A semi-deterministic modeling strategy was adopted by several authors [30,200–206] to study the combined effect of surface texture and roughness (multi-scale effects) under hydrodynamic and mixed lubrication conditions by solving the averaged Reynolds equation based on the Patir and Cheng model and mass-conservative cavitation. In these works, surface roughness effects (micro-scale) were treated through stochastic models (Patir and Cheng method for the lubricant flow and Greenwood-Williamson based models for asperity contact), while the surface textures (macro-scale) were considered deterministically through proper fine mesh discretization. Figure 16 summarizes the main aspects of different semi-deterministic models proposed in the literature to simulate rough textured surfaces.

Qiu and Khonsari [206] used a mass-conservative cavitation model to investigate the performance of textured dimples in seals and thrust bearings under mixed lubrication conditions. The authors verified the beneficial but minor effect of the surface roughness on the load carrying capacity of dimpled surfaces. It was also concluded that it exists an optimum dimple-to-diameter ratio and dimple density depending on the rotational speed for which the load carrying capacity is maximum. Moreover, it was verified that large dimple depths and increased roughness contribute towards higher seal leakage and that the friction force is decreased due to cavitation over the dimples. Similarly, Brunetière and Tournerie [207] showed that for smooth dimpled surfaces applied to mechanical seals, it is not possible to generate sufficient force to separate the surfaces, whereas a rough dimpled surface can significantly reduce friction.

The semi-deterministic model proposed by Profito et al. [30,203] was validated using experimental results obtained from a reciprocating test with groove surface texture. The same model was used

to explain the mechanisms associated with the transient effects induced by moving textures and their influence on the frictional response and film thickness variation in different lubrication regimes. Particularly, with respect to the boundary and mixed lubrication, it was shown that the interplay between inlet suction, asperity contact, cavitation, and fluid squeeze out all contribute to the frictional response and their relative contribution may differ depending on the operating regime. Furthermore, it was also discussed that under certain working conditions in mixed lubrication, as the textures move through the interface, the net effect of inlet suction and the subsequent fluid pressure boosting promoted by the fluid squeeze out tend to increase the film thickness and hence decrease the overall friction.

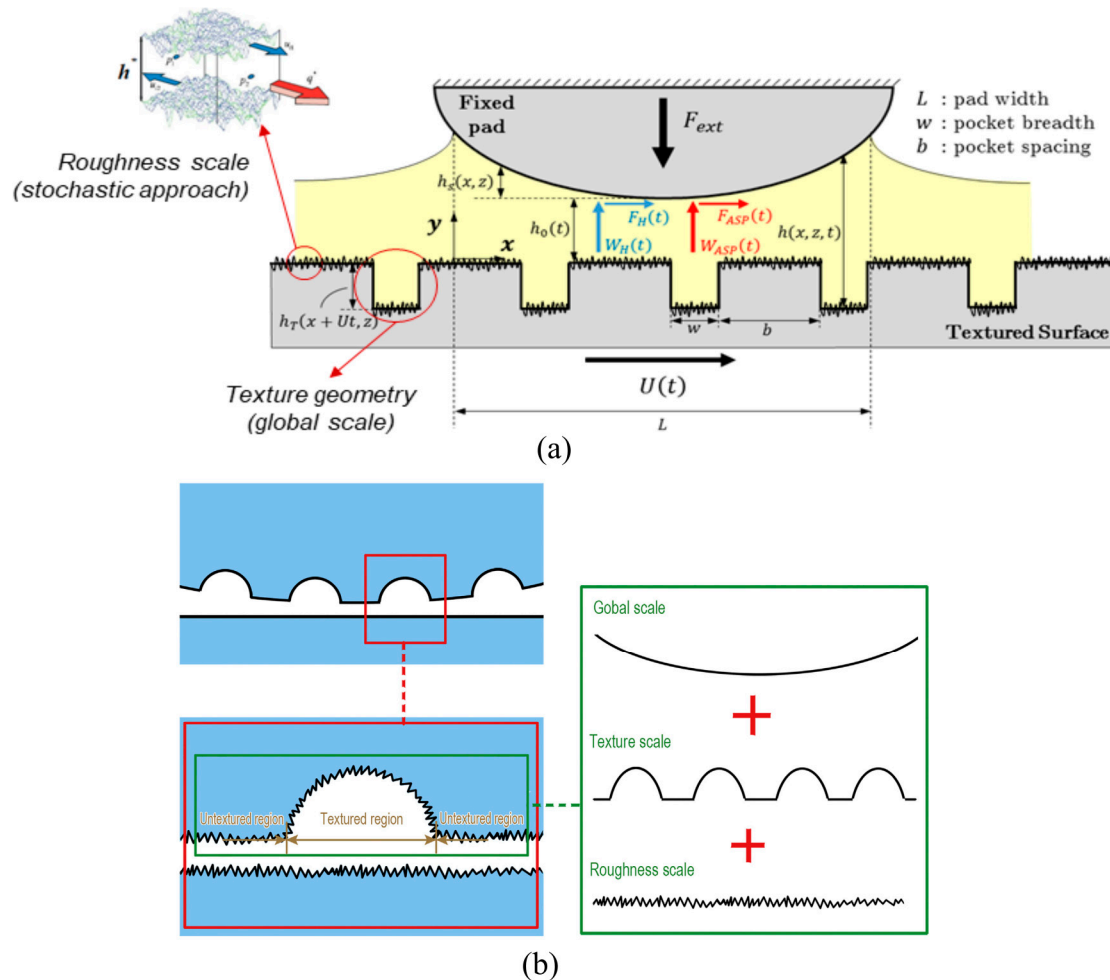


Figure 16. Examples of semi-deterministic models applied to simulate rough textured surfaces. In this modeling strategy, surface textures are considered deterministically, while surface roughness effects are taken into account through averaging (or homogenization) methods for lubricant flow and stochastic models for asperity contact. (a) Schematic of the rough contact interface with groove texture used by Profito et al. [30] to investigate the influence of the transient effects induced by moving textures on the frictional response and film thickness in different lubrication regimes. (b) Different scales of rough textured surfaces considered by Gu et al. [200] to study mixed lubrication problems in the presence of textures.

4.3. Numerical Multi-Scale Modeling

Finally, the third modeling approach which can be used to model multi-scale surface textures is based upon numerical multi-scale methods. It is important to emphasize that multi-scale modeling is not just about developing analytical models that use explicitly multi-physics coupling based upon the multi-scale expansion of the governing equations, it is also about developing numerical discretization

schemes and algorithms. Numerical multi-scale methods can be divided into two main classes [143]. The first class are algorithms conceived to efficiently solve the details of the problem, including the small-scale behavior. Examples of these methods applied to solve tribological problems are the multi-grid [208–213] and adaptive mesh refinements [214–218] methods. In fact, these are linear scaling algorithms, which implies that their computational complexity scales linearly with the number of degrees of freedom necessary to represent the detailed micro-scale solution. The second class is denoted domain decomposition, which provides a platform on which multi-scale methods can be constructed. In this case, the computational domain is divided into sub-domains and a simulation strategy is adopted based upon solving the given problem on each sub-domain, thus making sure that the solutions on different sub-domains match [143]. An important subclass of numerical multi-scale methods are numerical discretization schemes (e.g., finite element, finite volume or finite difference methods), which modify the finite discretization space to consider explicitly the micro-scale features of the problem. In other words, the finite discretization space is adapted by including functions with the proper micro-scale characteristics or by creating multi-scale basis functions that relate the micro- to macro-scale simulations [219–223]. A more in-depth understanding of numerical multi-scale methods for micro-meso-macroscopic scales coupling can be found in [143,144,224,225].

The use of multi-scale domain decomposition methods and multi-scale numerical discretization schemes to solve lubrication-related problems is not widely explored in the literature and has received attention only recently. However, especially due to the inherent sub-domain strategy of these methods, they are convenient and potentially powerful to deal with multi-scale surface textures. For instance, Pei et al. [226] developed a new finite cell method for modeling surface textures in hydrodynamic lubrication. This technique uses a matrix transformation reduction strategy in which the computational domain is divided into a fine-scale domain with texture cells and a coarser-scale domain without texture cells, as can be seen in Figure 17. The proposed methodology was compared with several test cases involving FEM, CFD, and existing theoretical and experimental data, thus demonstrating that both computing time and storage were significantly reduced. Afterwards, the same authors extended their multi-scale method to lubrication problems with rough surfaces considering parallel computation to speed-up the overall numerical solution. The results showed that the method can be used to predict the average mixed lubrication effects on the global scale (coarser mesh) from deterministic calculations in the small-scale, and to accurately recover the deterministic small-scale effects from the global scale results [227]. The same multi-scale methodology was then applied to investigate the influence of surface texture on the lubrication performance of floating ring bearings including thermal effects. Nine different texture patterns were analyzed, and the results verified that textures significantly increased the side leakage and reduced the temperature rise [228].

A multi-scale approach combining a micro-deterministic mixed lubrication model for small-scales and a macro-scale model was proposed by Nyemeck et al. [229,230] to predict the hydrodynamic load carrying capacity with nominally parallel surfaces. In this model, the mass flow conservation is ensured at the boundaries of micro-cells through the calculation of pressure variations at the macro-cell boundaries obtained from a micro-deterministic model with mass-conservative cavitation and asperity contact.

The classical homogenization approach applied to model mixed lubrication was extended by Pérez-Ràfols et al. [231] to study small flows by coupling two scales with a stochastic element. The proposed stochastic element is established using a two-scale formulation based upon the framework of the heterogeneous multi-scale method.

Two important advantages of this model is that (i) the periodic repetition of the topography is not assumed as in conventional homogenization methods, which allows using much smaller micro-scale domains, and (ii) the prediction of more realistic flow patterns compared with conventional homogenization models for similar small-scale domain size is possible. The multi-scale framework proposed by Gao and Hewson [194] was extended by de Boer et al. [232] to 3D micro-scale simulations and more accurate lubricant behavior. Particularly, a two-scale method using a heterogeneous

multi-scale approach to study the EHL and micro-EHL effects in tilted-pad bearings were developed. The micro-scale problem was solved by CFD simulations including surface elastic deformation, and a method for the homogenization of the micro-scale results was proposed and coupled to the macro-scale via pressure gradient-mass flow rate relationship.

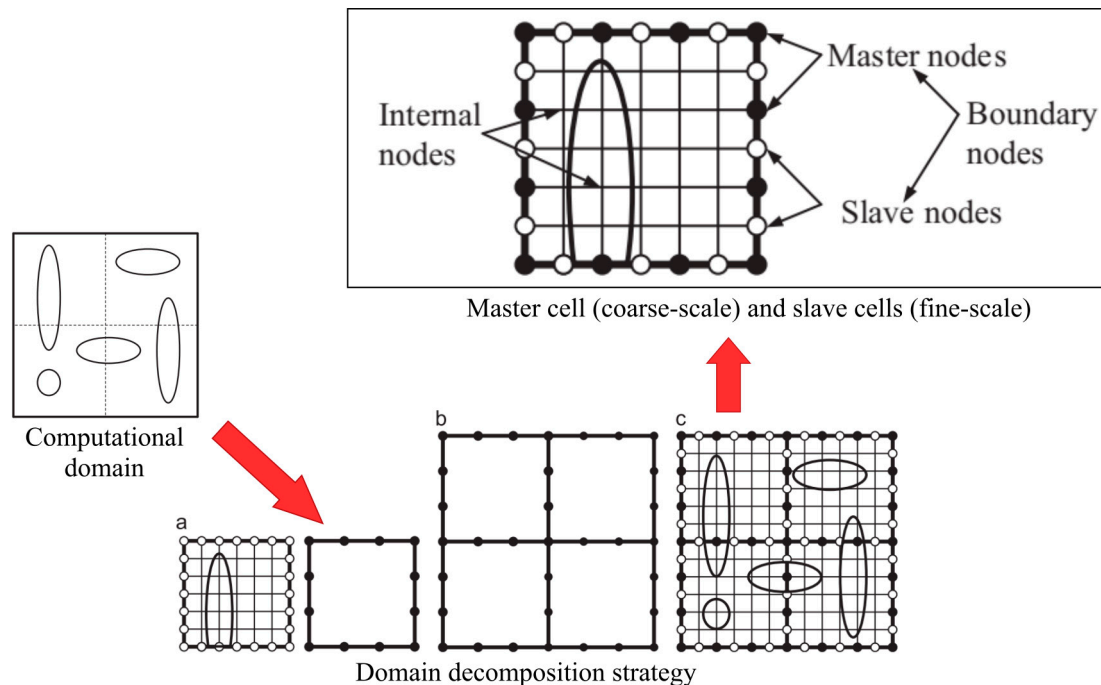


Figure 17. Overview of the finite cell method proposed by [227] for modeling surface textures in different lubrication regimes. (a) Illustration of the main domain decomposition steps and nomenclature of the proposed method.

More recently, Brunetière and Francisco [233] presented a multi-scale finite element method applied to the simulation of hydrodynamic lubrication of large rough contact surface. As illustrated in Figure 18a,b, the method is based on dividing the computational domain (macro-scale) into sub-domains (micro-scale) connected by a coarser mesh. The pressure distribution at the macro-scale is used as boundary conditions for the micro-scale problem, and then these boundary pressures are adjusted to guarantee the global mass flow conservation between contiguous sub-domains. A comparison between full deterministic and top-scale results with different values is shown in Figure 18c.

Finally, Costagliola et al. [234–237] proposed a spring-block modeling approach to investigate the fundamental mechanisms of dry friction between textured surfaces and how multi-scale surface textures influence static and dynamic friction. The model was used to show how the intricate surface geometry and local material properties on different length scales strongly affect the macroscopic friction force. Furthermore, it was also demonstrated how global friction properties can be tuned and optimized by designing composite surfaces with varying roughness features or local stiffness values.

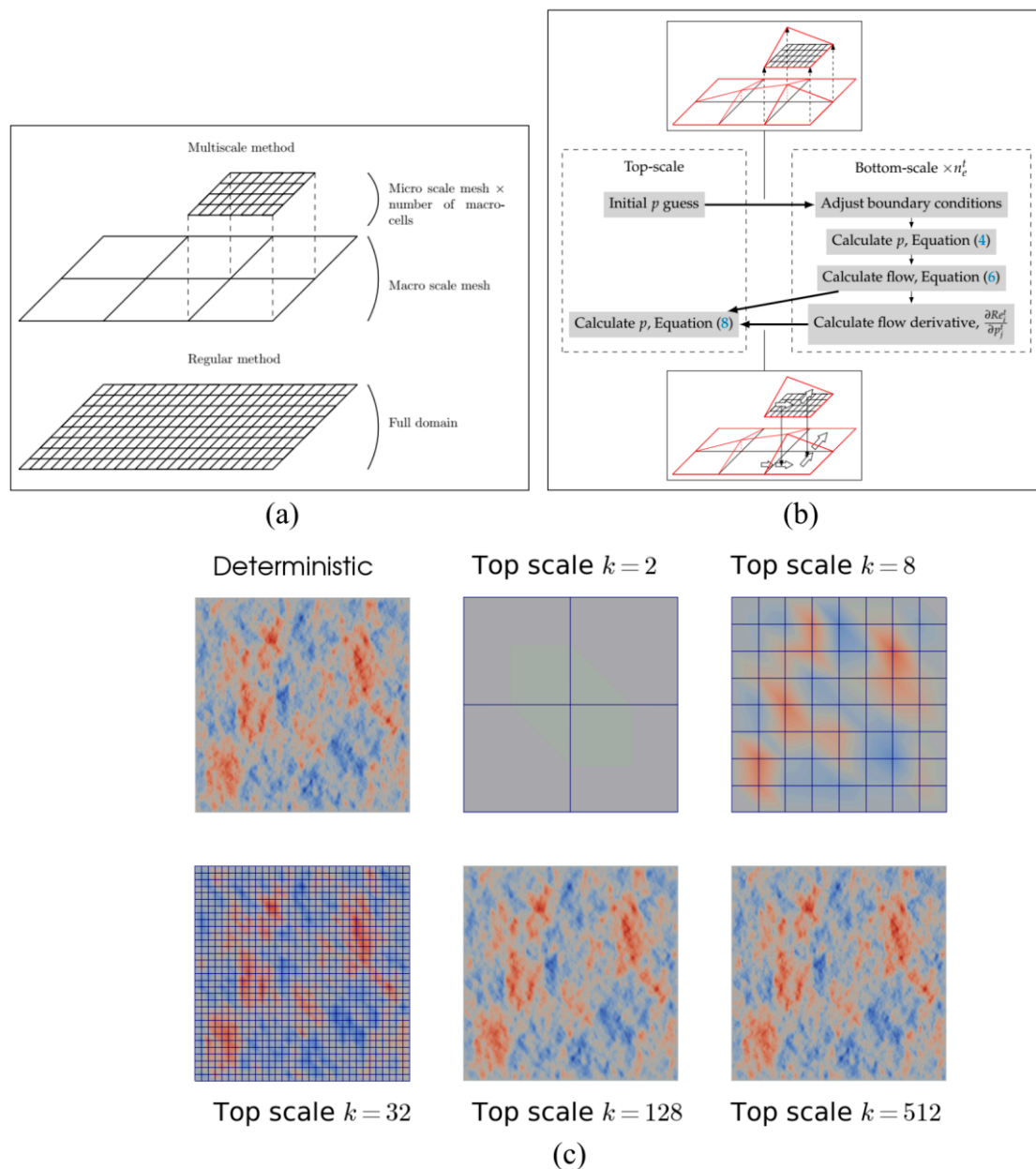


Figure 18. Overview of the multi-scale finite element method proposed by [233] to simulate hydrodynamic lubrication of large rough contact surfaces, which can be extended to deal with multi-scale textures. (a) Multi-scale mesh. (b) Multi-scale solution procedure. (c) Comparison between full deterministic and top-scale pressure distribution with different values.

5. Summary and Future Trends

This section summarizes the current knowledge and presents future trends regarding multi-scale surface textures applied to tribological problems. Even though several experimental and numerical works have tried to address the effects of multi-scale textures on friction and wear, the mechanisms responsible for the observed friction and wear reduction has not been fully identified yet. Therefore, we intend to derive some hypotheses regarding the underlying mechanisms for the improved tribological performance.

As already described in the introduction and depicted in Figure 19, surface textures may contribute to (i) increase the hydrodynamic pressure thus improving the load-carrying capacity (micro-hydrodynamic bearing effect) and reduce the shear-strain rate in the oil over the texture,

(ii) draw additional lubricant into the contact area (inlet-suction effect), (iii) store lubricant and supply it to the interface (oil reservoir effect), (iv) trap wear particles (debris trapping effect), and (v) reduce the real contact area thus reducing friction. Furthermore, under boundary and severe mixed lubrication conditions, surface textures may also affect sealing performance and percolation effects.

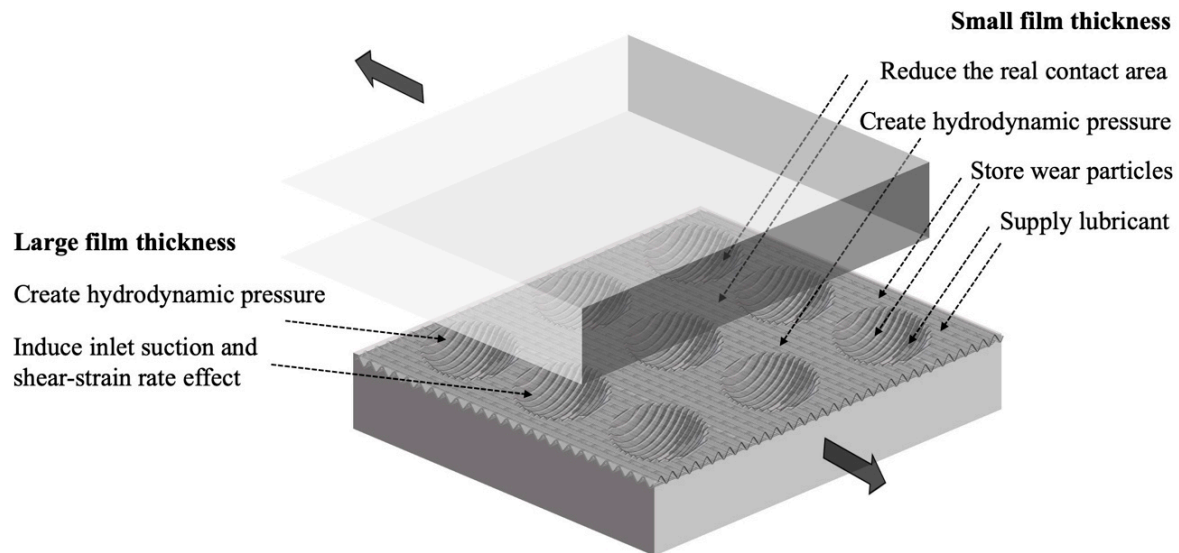


Figure 19. Schematic illustration of the possible mechanisms responsible for improved tribological performance of multi-scale surface textures. In this example, larger dimples with superimposed smaller cross-like textures are shown.

All the above-mentioned contributions are well known and accepted for single-scale textures. However, when taking multi-scale surface textures into consideration, it can be expected that a combination of different contributions may be responsible for superior friction and wear behavior. In this context, it is particularly important to simultaneously consider the type of contact (conformal or non-conformal), the operating conditions and the associated lubrication regime for the design of effective surface textures, since different mechanisms and design strategies need to be taken into consideration depending on the respective contact characteristics. Thereby, it must be emphasized that surface textures, which improve the tribological performance for specific conditions such as a certain range of film thicknesses or a specific lubrication regime, are not necessarily beneficial for all operating conditions [55]. It has been shown that beneficial surface textures optimized for a specific lubrication regime may even induce detrimental effects when used in another regime thus increasing friction and/or wear. In this sense, multi-scale surface textures pursue the goal to extend the range of operations conditions, in which a specific set of surface textures leads to superior tribological performance. This improves the general applicability of surface textures for industrial applications, since many machine elements operate under different lubrication regimes, sometimes even over a single operating cycle, as in piston and piston-ring cylinder liner contacts, connecting-rod bearings, gear meshing, cam-tapped systems among other.

For high-load and low-speed conditions inducing rather small film thicknesses (boundary lubrication), all texture types irrespective of the scale contribute to an improved frictional performance by reducing the real area of contact, supplying additional lubricant to the contact and trapping wear particles (reservoir effect). In this sense, multi-scale surfaces offer the advantage of having a greater surface area covered with textures in which a potentially higher volume of lubricant and wear particles can be stored. However, the combination of low film thickness and small features can also weaken surface integrity due to induced edge effects and stress raisers thus accelerating wear processes. [238,239]. At intermediate load and speed conditions (mixed lubrication), the lubricant film starts to partially carry the applied load. For these conditions, especially shallow textures with

rather low depths tend to increase the hydrodynamic pressure and therefore improve the overall frictional behavior. It has been numerically and experimentally shown that when the structural depth is in the same range as the resulting lubricant film thickness, the greatest effects in terms of an additional pressure build-up can be expected [21,34,36,240]. In this regard, under mixed lubrication conditions, multi-scale surfaces can increase the hydrodynamic pressure due to small texture features and, additionally, offer the advantage to provide a great reservoir volume for lubricant and wear debris. Finally, at high lubricant film thicknesses for which the load is mostly carried by the oil, mainly larger texture features improve the frictional performance by increasing the hydrodynamic pressure (inlet suction mechanism and reducing of oil shear-strain rate) thus reducing the transition speed from mixed to hydrodynamic lubrication [93]. Furthermore, it can be assumed that smaller textures have a negligible effect in this lubrication regime. Hence, while not improving the tribological properties compared to single-scale textures, in this case, multi-scale surfaces can still perform well in this lubrication regime.

Summarizing, it can be stated that multi-scale surfaces can have a synergetic effect when suitably combined thus reducing friction and wear over a broader range of operating conditions. To fully use the advantages of multi-scale surface textures, they must be carefully and properly designed. Under hydrodynamic lubrication, this comprises maximizing the hydrodynamic pressure and/or reduce leakage flow without inducing negative effects due to pronounced cavitation or flow circulation problems inside bigger texture features. For mixed lubrication with a significant solid-solid contact (small film thicknesses), textures should be designed in a way that the advantages of an additional hydrodynamic pressure induced by the shallow features overcompensate potential negative effects induced by pronounced cavitation, flow circulation or edge effects (stress raisers) [21, 241,242]. Additionally, smaller and more densely distributed textures may also lead to improved wetting behavior and a better lubricant's distribution in the contact zone, which can help to reduce cavitation and flow circulation thus ultimately improving the load-carrying capacity. Nevertheless, it must be stressed that more fundamental studies will be needed to properly evaluate important parameters in multi-scale textures. In this context, it has already been demonstrated that certain geometrical parameters, such as the aspect ratio, the area density, and their ratio to the texture size, determine the tribological behavior of single-scale surface textures. A comprehensive overview of beneficial single-scale texture geometries under different speed and load conditions can be found in the review presented by Gachot et al. [22]. Moreover, the relation between the acting oil thickness and the involved scales (depths) in multi-scale textures needs to be investigated systematically.

Numerical modeling of the tribological behavior of multi-scale textures is considered to be a powerful tool to optimize the design of multi-scale textures since this approach is more time-efficient and less costly thus reducing the well-practiced trial-and-error methodology. However, it should be emphasized that it is always desirable to cross-correlate the obtained numerical results with experimental data to validate and further improve the mathematical models and optimize the overall design process of multi-scale textures. Since cavitation and the lubricant's flow and distribution in the contact zone play an important role, one interesting approach would be to design tribological experiments with multi-scale textured samples allowing the imaging of the contact zone (in- or ex-situ) and/or the measurement of the lubricant film thickness, the fluid flow velocity, and temperature distributions.

Moreover, modeling and simulation should be further integrated into the design process. In this context, the future trends regarding modeling and simulation of surface textures reside on the continuous development and consolidation of virtual simulation tools, which smartly combine:

- (i) the modeling approaches previously described to accurately predict the tribological behavior of textured surfaces under different lubrication regimes,
- (ii) optimization techniques and, potentially, the use of machine learning algorithms to speed-up the determination of optimum texture designs for friction and wear reduction in different applications,
- (iii) the exploration of nature-inspired multi-scale textures for tribological applications.

The development of this computational surface engineering framework can be structured according to the following aspects:

- (1) The effect of surface texture on the global, component-size scale would be determined on the basis of well-posed analytical multi-scale methods. Good candidates are the Patir and Cheng average flow model [151,152], the micro-macro method of de Kraker et al. [155,156], as well as the homogenization techniques proposed by Almqvist [176–185], Scaraggi [189–193] and the extension of Wassem et al. [197,198] and Yildiran et al. [199] models to mixed lubrication.
- (2) Proper calculation of flow factor (or homogenization) tensors using full deterministic simulations. In this case, an extension of the Hu and Zhu mixed-TEHL model [111,114,115,117,121,126] by including mass-conservative cavitation and advanced rheological models for better predictions of the shear flow factor tensors would be a good alternative.
- (3) Use of powerful computational techniques and algorithms, such as multi-grid methods and parallel computing, to speed up deterministic simulations for the determination of flow factor tensors.
- (4) Explore the use of numerical multi-scale methods, such as domain decomposition methods and numerical discretization schemes, to model and simulate lubrication problems with multi-scale surface textures.
- (5) Development of a computational surface engineering simulation framework as an open source project available to the entire tribology community. Furthermore, the construction of an open source library for storing the flow factors and other important simulation parameters obtained from previously simulated surface textures would be helpful, which, in turn, could be used to accelerate the innovative texture design and optimization for a wide range of surface textures.

Summarizing, numerical methods and experiments should be suitably combined to further push the development and design of multi-scale surfaces to enable lower friction and wear over a broader range of tribological conditions. By doing so, optimized designs such as new texture geometries and multi-scale textures being comprised of features on more than two scales can be tested. Additionally, texturing techniques, which enable the fabrication of multi-scale surfaces should be subject to further investigation. In this context, techniques with many degrees of freedom to create new interesting shapes and efficient techniques, thus paving the way to mass production, are interesting. Gaining more knowledge about the potential tribological effects of multi-scale surface texture combined with the possibility to fabricate more sophisticated texture arrangement can also boost the application side in the future. Having the beneficial effects of multi-scale textures in journal bearings in mind, as outlined in Section 3, it can be imagined that this can be just the beginning of the journey. Multi-scale textures seem to be very promising to improve the friction and wear characteristics in the piston ring cylinder liner contacts. In this regard, textures on different scales could be designed appropriately to enable beneficial frictional properties along the entire stroke irrespective of the sliding velocity. Other machine components, which could significantly benefit from the usage of multi-scale surface textures, are cam followers, rolling element bearings, thrust and sliding bearings among others.

Author Contributions: P.G.G., F.J.P. and A.R. contributed equally regarding the manuscript's conception, the literature review, the manuscript's writing as well as its proof-reading.

Funding: A. Rosenkranz gratefully acknowledges the financial support given by CONICYT in the framework of the project (Fondecyt Iniciación 11180121). In addition, A. Rosenkranz would like to acknowledge the VID for the financial support given in the project UI 013/2018.

Conflicts of Interest: The authors declare no conflict of interest.

References

1. Dowson, D. *History of Tribology*; Longman: London, UK, 1979; ISBN 978-0-582-44766-0.
2. Williams, J. *Engineering Tribology*; Cambridge University Press: Cambridge, UK, 2005; ISBN 9780511805905.
3. Amontons, G. De la résistance causée dans les machines. *Mémoires l'Académie R. A* **1699**, 257–282.

4. Gao, J.; Luedtke, W.D.; Gourdon, D.; Ruths, M.; Israelachvili, J.N.; Landman, U. Frictional forces and Amontons' law: From the molecular to the macroscopic scale. *J. Phys. Chem. B* **2004**, *108*, 3410–3425. [[CrossRef](#)]
5. Bowden, F.P.; Tabor, D. Mechanism of metallic friction. *Nature* **1942**, *150*, 197–199. [[CrossRef](#)]
6. Archard, J.F. Contact and rubbing of flat surfaces. *J. Appl. Phys.* **1953**, *24*, 981–988. [[CrossRef](#)]
7. Greenwood, J.A.; Williamson, J.B.P. Contact of Nominally Flat Surfaces. *Proc. R. Soc. A Math. Phys. Eng. Sci.* **1966**, *295*, 300–319.
8. Nosonovsky, M.; Bhushan, B. *Multiscale Dissipative Mechanisms and Hierarchical Surfaces*; NanoScience and Technology; Springer: Berlin/Heidelberg, Germany, 2008; ISBN 978-3-540-78424-1.
9. Liu, Z.; Yin, W.; Tao, D.; Tian, Y. A glimpse of superb tribological designs in nature. *Biotribology* **2015**, *1*, 11–23. [[CrossRef](#)]
10. Malshe, A.P.; Bapat, S.; Rajurkar, K.P.; Haitjema, H. Bio-inspired textures for functional applications. *CIRP Ann.* **2018**, *67*, 627–650. [[CrossRef](#)]
11. Guo, Y.; Zhang, Z.; Zhang, S. Advances in the application of biomimetic surface engineering in the oil and gas industry. *Friction* **2019**, *7*, 289–306. [[CrossRef](#)]
12. Dean, B.; Bhushan, B. Shark-skin surfaces for fluid-drag reduction in turbulent flow: A review. *Philos. Trans. R. Soc. A Math. Phys. Eng. Sci.* **2010**, *368*, 4775–4806. [[CrossRef](#)]
13. Bixler, G.D.; Bhushan, B. Fluid drag reduction with shark-skin riblet inspired microstructured surfaces. *Adv. Funct. Mater.* **2013**, *23*, 4507–4528. [[CrossRef](#)]
14. Greiner, C.; Arzt, E.; Del Campo, A. Hierarchical gecko-like adhesives. *Adv. Mater.* **2009**, *21*, 479–482. [[CrossRef](#)]
15. Murphy, M.P.; Kim, S.; Sitti, M. Enhanced adhesion by gecko-inspired hierarchical fibrillar adhesives. *ACS Appl. Mater. Interfaces* **2009**, *1*, 849–855. [[CrossRef](#)] [[PubMed](#)]
16. Sun, J.; Bhushan, B. Nanomanufacturing of bioinspired surfaces. *Tribol. Int.* **2019**, *129*, 67–74. [[CrossRef](#)]
17. Koch, K.; Bhushan, B.; Jung, Y.C.; Barthlott, W. Fabrication of artificial Lotus leaves and significance of hierarchical structure for superhydrophobicity and low adhesion. *Soft Matter* **2009**, *5*, 1386. [[CrossRef](#)]
18. Lin, J.; Cai, Y.; Wang, X.; Ding, B.; Yu, J.; Wang, M. Fabrication of biomimetic superhydrophobic surfaces inspired by lotus leaf and silver ragwort leaf. *Nanoscale* **2011**, *3*, 1258–1262. [[CrossRef](#)]
19. Etsion, I. Improving tribological performance of mechanical components by laser surface texturing. *Tribol. Lett.* **2004**, *17*, 733–737. [[CrossRef](#)]
20. Etsion, I. State of the Art in Laser Surface Texturing. *J. Tribol.* **2005**, *127*, 248–253. [[CrossRef](#)]
21. Gropper, D.; Wang, L.; Harvey, T.J. Hydrodynamic lubrication of textured surfaces: A review of modeling techniques and key findings. *Tribol. Int.* **2016**, *94*, 509–529. [[CrossRef](#)]
22. Gachot, C.; Rosenkranz, A.; Hsu, S.M.; Costa, H.L. A critical assessment of surface texturing for friction and wear improvement. *Wear* **2017**, *372–373*, 21–41. [[CrossRef](#)]
23. Rosenkranz, A.; Grützmacher, P.G.; Gachot, C.; Costa, H.L. Surface Texturing in Machine Elements—A Critical Discussion for Rolling and Sliding Contacts. *Adv. Eng. Mater.* **2019**, *21*, 1900194. [[CrossRef](#)]
24. Sudeep, U.; Tandon, N.; Pandey, R.K. Performance of Lubricated Rolling/Sliding Concentrated Contacts With Surface Textures: A Review. *J. Tribol.* **2015**, *137*, 031501. [[CrossRef](#)]
25. Rosenkranz, A.; Costa, H.L.; Profito, F.; Gachot, C.; Medina, S.; Dini, D. Influence of surface texturing on hydrodynamic friction in plane converging bearings—An experimental and numerical approach. *Tribol. Int.* **2019**, *134*, 190–204. [[CrossRef](#)]
26. Costa, H.L.; Hutchings, I.M. Hydrodynamic lubrication of textured steel surfaces under reciprocating sliding conditions. *Tribol. Int.* **2007**, *40*, 1227–1238. [[CrossRef](#)]
27. Fowell, M.; Olver, A.V.; Gosman, A.D.; Spikes, H.A.; Pegg, I. Entrainment and Inlet Suction: Two Mechanisms of Hydrodynamic Lubrication in Textured Bearings. *J. Tribol.* **2007**, *129*, 336. [[CrossRef](#)]
28. Fowell, M.T.; Medina, S.; Olver, A.V.; Spikes, H.A.; Pegg, I.G. Parametric study of texturing in convergent bearings. *Tribol. Int.* **2012**, *52*, 7–16. [[CrossRef](#)]
29. Vlădescu, S.C.; Ciniero, A.; Tufail, K.; Gangopadhyay, A.; Reddyhoff, T. Looking into a laser textured piston ring-liner contact. *Tribol. Int.* **2017**, *115*, 140–153. [[CrossRef](#)]
30. Profito, F.J.; Vlădescu, S.C.; Reddyhoff, T.; Dini, D. Transient experimental and modelling studies of laser-textured micro-grooved surfaces with a focus on piston-ring cylinder liner contacts. *Tribol. Int.* **2017**, *113*, 125–136. [[CrossRef](#)]

31. Dobrica, M.B.; Fillon, M.; Pascovici, M.D.; Cicone, T. Optimizing surface texture for hydrodynamic lubricated contacts using a mass-conserving numerical approach. *Proc. Inst. Mech. Eng. Part J J. Eng. Tribol.* **2010**, *224*, 737–750. [[CrossRef](#)]
32. Erdemir, A. Review of engineered tribological interfaces for improved boundary lubrication. *Tribol. Int.* **2005**, *38*, 249–256. [[CrossRef](#)]
33. Pettersson, U.; Jacobson, S. Influence of surface texture on boundary lubricated sliding contacts. *Tribol. Int.* **2003**, *36*, 857–864. [[CrossRef](#)]
34. Rosenkranz, A.; Heib, T.; Gachot, C.; Mücklich, F. Oil film lifetime and wear particle analysis of laser-patterned stainless steel surfaces. *Wear* **2015**, *334–335*, 1–12. [[CrossRef](#)]
35. Braun, D.; Greiner, C.; Schneider, J.; Gumbsch, P. Efficiency of laser surface texturing in the reduction of friction under mixed lubrication. *Tribol. Int.* **2014**, *77*, 142–147. [[CrossRef](#)]
36. Ramesh, A.; Akram, W.; Mishra, S.P.; Cannon, A.H.; Polycarpou, A.A.; King, W.P. Friction characteristics of microtextured surfaces under mixed and hydrodynamic lubrication. *Tribol. Int.* **2013**, *57*, 170–176. [[CrossRef](#)]
37. Gachot, C.; Rosenkranz, A.; Reinert, L.; Ramos-Moore, E.; Souza, N.; Müser, M.H.; Mücklich, F. Dry friction between laser-patterned surfaces: Role of alignment, structural wavelength and surface chemistry. *Tribol. Lett.* **2013**, *49*, 193–202. [[CrossRef](#)]
38. Rosenkranz, A.; Reinert, L.; Gachot, C.; Mücklich, F. Alignment and wear debris effects between laser-patterned steel surfaces under dry sliding conditions. *Wear* **2014**, *318*, 49–61. [[CrossRef](#)]
39. Prodanov, N.; Gachot, C.; Rosenkranz, A.; Mücklich, F.; Müser, M.H. Contact mechanics of laser-textured surfaces: Correlating contact area and friction. *Tribol. Lett.* **2013**, *50*, 41–48. [[CrossRef](#)]
40. Abdel-Aal, H.A. Functional surfaces for tribological applications: Inspiration and design. *Surf. Topogr. Metrol. Prop.* **2016**, *4*, 1–37. [[CrossRef](#)]
41. Costa, H.L.L.; Hutchings, I.M. Some innovative surface texturing techniques for tribological purposes. *Proc. Inst. Mech. Eng. Part J J. Eng. Tribol.* **2015**, *229*, 429–448. [[CrossRef](#)]
42. Coblas, D.G.; Fatu, A.; Maoui, A.; Hajjam, M. Manufacturing textured surfaces: State of art and recent developments. *Proc. Inst. Mech. Eng. Part J J. Eng. Tribol.* **2015**, *229*, 3–29. [[CrossRef](#)]
43. Abdel-Aal, H.A.; El Mansori, M. Tribological analysis of the ventral scale structure in a Python regius in relation to laser textured surfaces. *Surf. Topogr. Metrol. Prop.* **2013**, *1*. [[CrossRef](#)]
44. Wang, Y.; Yang, J.; Guo, X.; Zhang, Q.; Wang, J.; Ding, J.; Yuan, N. Fabrication and tribological properties of superhydrophobic nickel films with positive and negative biomimetic microtextures. *Friction* **2014**, *2*, 287–294. [[CrossRef](#)]
45. Shafiei, M.; Alpas, A.T. Fabrication of biotextured nanocrystalline nickel films for the reduction and control of friction. *Mater. Sci. Eng. C* **2008**, *28*, 1340–1346. [[CrossRef](#)]
46. Shafiei, M.; Alpas, A.T. Nanocrystalline nickel films with lotus leaf texture for superhydrophobic and low friction surfaces. *Appl. Surf. Sci.* **2009**, *256*, 710–719. [[CrossRef](#)]
47. Resendiz, J.; Egberts, P.; Park, S.S. Tribological Behavior of Multi-scaled Patterned Surfaces Machined Through Inclined End Milling and Micro Shot Blasting. *Tribol. Lett.* **2018**, *66*, 132. [[CrossRef](#)]
48. Grützmacher, P.G.; Rosenkranz, A.; Szurdak, A.; Gachot, C.; Hirt, G.; Mücklich, F. Effects of Multi-Scale Patterning on the Run-In Behavior of Steel-Alumina Pairings under Lubricated Conditions. *Adv. Eng. Mater.* **2018**, *20*, 1700521. [[CrossRef](#)]
49. Grützmacher, P.G.; Rosenkranz, A.; Szurdak, A.; Gachot, C.; Hirt, G.; Mücklich, F. Lubricant migration on stainless steel induced by bio-inspired multi-scale surface patterns. *Mater. Des.* **2018**, *150*, 55–63. [[CrossRef](#)]
50. Rukosuyev, M.V.; Lee, J.; Cho, S.J.; Lim, G.; Jun, M.B.G.G. One-step fabrication of superhydrophobic hierarchical structures by femtosecond laser ablation. *Appl. Surf. Sci.* **2014**, *313*, 411–417. [[CrossRef](#)]
51. Jagdheesh, R.; García-Ballesteros, J.J.; Ocaña, J.L. One-step fabrication of near superhydrophobic aluminum surface by nanosecond laser ablation. *Appl. Surf. Sci.* **2015**, *374*, 2–11. [[CrossRef](#)]
52. Martínez-Calderon, M.; Rodríguez, A.; Dias-Ponte, A.; Morant-Miñana, M.C.C.; Gómez-Aranzadi, M.; Olaizola, S.M.M. Femtosecond laser fabrication of highly hydrophobic stainless steel surface with hierarchical structures fabricated by combining ordered microstructures and LIPSS. *Appl. Surf. Sci.* **2016**, *374*, 81–89. [[CrossRef](#)]
53. Long, J.; Fan, P.; Zhong, M.; Zhang, H.; Xie, Y.; Lin, C. Superhydrophobic and colorful copper surfaces fabricated by picosecond laser induced periodic nanostructures. *Appl. Surf. Sci.* **2014**, *311*, 461–467. [[CrossRef](#)]

54. Gachot, C.; Rosenkranz, A.; Wietbrock, B.; Hirt, G.; Mücklich, F. Advanced Design of Hierarchical Topographies in Metallic Surfaces by Combining Micro-Coining and Laser Interference Patterning. *Adv. Eng. Mater.* **2013**, *15*, 503–509. [[CrossRef](#)]
55. Hsu, S.M.; Jing, Y.; Zhao, F. Self-adaptive surface texture design for friction reduction across the lubrication regimes. *Surf. Topogr. Metrol. Prop.* **2016**, *4*, 014004. [[CrossRef](#)]
56. Sugioka, K.; Meunier, M.; Piqué, A. (Eds.) *Laser Precision Microfabrication*; Springer Series in Materials Science; Springer: Berlin/Heidelberg, Germany, 2010; Volume 135, ISBN 978-3-642-10522-7.
57. Vorobyev, A.Y.; Guo, C. Direct femtosecond laser surface nano/microstructuring and its applications. *Laser Photonics Rev.* **2013**, *7*, 385–407. [[CrossRef](#)]
58. Marczak, J. Micromachining And Patterning In Micro/Nano Scale On Macroscopic Areas. *Arch. Metall. Mater.* **2015**, *60*, 2221–2234. [[CrossRef](#)]
59. Kirner, S.V.; Hermens, U.; Mimidis, A.; Skoulas, E.; Florian, C.; Hischen, F.; Plamadeala, C.; Baumgartner, W.; Winands, K.; Mescheder, H.; et al. Mimicking bug-like surface structures and their fluid transport produced by ultrashort laser pulse irradiation of steel. *Appl. Phys. A Mater. Sci. Process.* **2017**, *123*, 1–13. [[CrossRef](#)]
60. Hermens, U.; Kirner, S.V.; Emonts, C.; Comanns, P.; Skoulas, E.; Mimidis, A.; Mescheder, H.; Winands, K.; Krüger, J.; Stratakis, E.; et al. Mimicking lizard-like surface structures upon ultrashort laser pulse irradiation of inorganic materials. *Appl. Surf. Sci.* **2017**, *418*, 499–507. [[CrossRef](#)]
61. Neuenschwander, B.; Jaeggi, B.; Schmid, M.; Hennig, G. Surface Structuring with Ultra-short Laser Pulses: Basics, Limitations and Needs for High Throughput. *Phys. Procedia* **2014**, *56*, 1047–1058. [[CrossRef](#)]
62. Mücklich, F.; Lasagni, A.F.; Daniel, C. Laser interference metallurgy—Using interference as a tool for micro/nano structuring. *Int. J. Mater. Res.* **2006**, *97*, 1337–1344. [[CrossRef](#)]
63. Leitz, K.-H.; Redlingshöfer, B.; Reg, Y.; Otto, A.; Schmidt, M. Metal Ablation with Short and Ultrashort Laser Pulses. *Phys. Procedia* **2011**, *12*, 230–238. [[CrossRef](#)]
64. Segu, D.Z.; Hwang, P. Effectiveness of multi-shape laser surface texturing in the reduction of friction under lubrication regime. *Ind. Lubr. Tribol.* **2016**, *68*, 116–124. [[CrossRef](#)]
65. Segu, D.Z.; Choi, S.G.; Choi, J.H.; Kim, S.S. The effect of multi-scale laser textured surface on lubrication regime. *Appl. Surf. Sci.* **2013**, *270*, 58–63. [[CrossRef](#)]
66. Zenebe Segu, D.; Hwang, P. Friction control by multi-shape textured surface under pin-on-disc test. *Tribol. Int.* **2015**, *91*, 111–117. [[CrossRef](#)]
67. Kwon, Y.; Patankar, N.; Choi, J.; Lee, J. Design of surface hierarchy for extreme hydrophobicity. *Langmuir* **2009**, *25*, 6129–6136. [[CrossRef](#)] [[PubMed](#)]
68. Rupp, F.; Scheideler, L.; Rehbein, D.; Axmann, D.; Geis-Gerstorfer, J. Roughness induced dynamic changes of wettability of acid etched titanium implant modifications. *Biomaterials* **2004**, *25*, 1429–1438. [[CrossRef](#)] [[PubMed](#)]
69. Rosenkranz, A.; Grützmacher, P.G.; Szurdak, A.; Gachot, C.; Hirt, G.; Mücklich, F.; Muecklich, F. Synergetic effect of laser patterning and micro coining for controlled lubricant propagation. *Surf. Topogr. Metrol. Prop.* **2016**, *4*, 034008. [[CrossRef](#)]
70. Rosenkranz, A.; Grützmacher, P.G.; Murzyn, K.; Mathieu, C.; Mücklich, F. Multi-scale surface patterning to tune friction under mixed lubricated conditions. *Appl. Nanosci.* **2019**. [[CrossRef](#)]
71. Grützmacher, P.G.; Rosenkranz, A.; Szurdak, A.; Grüber, M.; Gachot, C.; Hirt, G.; Mücklich, F. Multi-scale surface patterning—An approach to control friction and lubricant migration in lubricated systems. *Ind. Lubr. Tribol.* **2019**, *71*, 1007–1016. [[CrossRef](#)]
72. Grützmacher, P.G.; Rosenkranz, A.; Szurdak, A.; König, F.; Jacobs, G.; Hirt, G.; Mücklich, F. From lab to application—Improved frictional performance of journal bearings induced by single- and multi-scale surface patterns. *Tribol. Int.* **2018**, *127*, 500–508. [[CrossRef](#)]
73. Kim, M.; Lee, S.M.; Lee, S.J.; Kim, Y.W.; Lee, D.W. Effect on friction reduction of micro/nano hierarchical patterns on sapphire wafers. *Int. J. Precis. Eng. Manuf.-Green Technol.* **2017**, *4*, 27–35. [[CrossRef](#)]
74. Akkan, C.K.; Hammadeh, M.E.; May, A.; Park, H.W.; Abdul-Khaliq, H.; Strunskus, T.; Aktas, O.C. Surface topography and wetting modifications of PEEK for implant applications. *Lasers Med. Sci.* **2014**, *29*, 1633–1639. [[CrossRef](#)]
75. Fürstner, R.; Barthlott, W.; Neinhuis, C.; Walzel, P. Wetting and self-cleaning properties of artificial superhydrophobic surfaces. *Langmuir* **2005**, *21*, 956–961. [[CrossRef](#)] [[PubMed](#)]

76. Cardoso, J.T.; Aguilar-Morales, A.I.; Alamri, S.; Huerta-Murillo, D.; Cordovilla, F.; Lasagni, A.F.; Ocaña, J.L. Superhydrophobicity on hierarchical periodic surface structures fabricated via direct laser writing and direct laser interference patterning on an aluminium alloy. *Opt. Lasers Eng.* **2018**, *111*, 193–200. [[CrossRef](#)]
77. Huerta-Murillo, D.; Aguilar-Morales, A.I.; Alamri, S.; Cardoso, J.T.; Jagdheesh, R.; Lasagni, A.F.; Ocaña, J.L. Fabrication of multi-scale periodic surface structures on Ti-6Al-4V by direct laser writing and direct laser interference patterning for modified wettability applications. *Opt. Lasers Eng.* **2017**, *98*, 134–142. [[CrossRef](#)]
78. Zhang, K.; Deng, J.; Guo, X.; Sun, L.; Lei, S. Study on the adhesion and tribological behavior of PVD TiAlN coatings with a multi-scale textured substrate surface. *Int. J. Refract. Met. Hard Mater.* **2018**, *72*, 292–305. [[CrossRef](#)]
79. Bhushan, B.; Koch, K.; Jung, Y.C. Nanostructures for superhydrophobicity and low adhesion. *Soft Matter* **2008**, *4*, 1799. [[CrossRef](#)]
80. Zhang, F.; Low, H.Y. Anisotropic wettability on imprinted hierarchical structures. *Langmuir* **2007**, *23*, 7793–7798. [[CrossRef](#)]
81. Tanvir Ahmed, K.M.; Kietzig, A.M. Drag reduction on laser-patterned hierarchical superhydrophobic surfaces. *Soft Matter* **2016**, *12*, 4912–4922. [[CrossRef](#)]
82. Qiu, R.; Wang, P.; Zhang, D.; Wu, J. One-step preparation of hierarchical cobalt structure with inborn superhydrophobic effect. *Colloids Surf. A Physicochem. Eng. Asp.* **2011**, *377*, 144–149. [[CrossRef](#)]
83. Wu, B.; Zhou, M.; Li, J.; Ye, X.; Li, G.; Cai, L. Superhydrophobic surfaces fabricated by microstructuring of stainless steel using a femtosecond laser. *Appl. Surf. Sci.* **2009**, *256*, 61–66. [[CrossRef](#)]
84. Wang, Y.; Wang, L.; Wang, S.; Wood, R.J.K.; Xue, Q. From natural lotus leaf to highly hard-flexible diamond-like carbon surface with superhydrophobic and good tribological performance. *Surf. Coat. Technol.* **2012**, *206*, 2258–2264. [[CrossRef](#)]
85. Abdel-Aal, H.A.; El Mansori, M.; Mezghani, S. Multi-scale investigation of surface topography of ball python (*python regius*) shed skin in comparison to human skin. *Tribol. Lett.* **2010**, *37*, 517–527. [[CrossRef](#)]
86. Abdel-Aal, H.A.; Vargiolu, R.; Zahouani, H.; El Mansori, M. A study on the frictional response of reptilian shed skin. *J. Phys. Conf. Ser.* **2011**, *311*, 012016. [[CrossRef](#)]
87. Cuervo, P.; López, D.A.; Cano, J.P.; Sánchez, J.C.; Rudas, S.; Estupiñán, H.; Toro, A.; Abdel-Aal, H.A. Development of low friction snake-inspired deterministic textured surfaces. *Surf. Topogr. Metrol. Prop.* **2016**, *4*, 1–17. [[CrossRef](#)]
88. Greiner, C.; Schäfer, M. Bio-inspired scale-like surface textures and their tribological properties. *Bioinspiration Biomim.* **2015**, *10*, 44001. [[CrossRef](#)] [[PubMed](#)]
89. Schneider, J.; Djamiykov, V.; Greiner, C. Friction reduction through biologically inspired scale-like laser surface textures. *Beilstein J. Nanotechnol.* **2018**, *9*, 2561–2572. [[CrossRef](#)]
90. Wang, X.; Kato, K.; Adachi, K.; Aizawa, K. Loads carrying capacity map for the surface texture design of SiC thrust bearing sliding in water. *Tribol. Int.* **2003**, *36*, 189–197. [[CrossRef](#)]
91. Wang, X.; Adachi, K.; Otsuka, K.; Kato, K. Optimization of the surface texture for silicon carbide sliding in water. *Appl. Surf. Sci.* **2006**, *253*, 1282–1286. [[CrossRef](#)]
92. Yu, H.; Huang, W.; Wang, X. Dimple patterns design for different circumstances. *Lubr. Sci.* **2013**, *25*, 67–78. [[CrossRef](#)]
93. Hsu, S.M.; Jing, Y.; Hua, D.; Zhang, H. Friction reduction using discrete surface textures: Principle and design. *J. Phys. D. Appl. Phys.* **2014**, *47*, 335307. [[CrossRef](#)]
94. Rosenkranz, A.; Szurdak, A.; Gachot, C.; Hirt, G.; Mücklich, F. Friction reduction under mixed and full film EHL induced by hot micro-coined surface patterns. *Tribol. Int.* **2016**, *95*, 290–297. [[CrossRef](#)]
95. Choi, H.; Moin, P.; Kim, J. Direct numerical simulation of turbulent flow over riblets. *J. Fluid Mech.* **1993**, *255*, 503. [[CrossRef](#)]
96. Choi, H.; Moin, P.; Kim, J. Active turbulence control for drag reduction in wall-bounded flows. *J. Fluid Mech.* **1994**, *262*, 75–110. [[CrossRef](#)]
97. Zhang, D.; Luo, Y.; Li, X.; Chen, H. Numerical Simulation and Experimental Study of Drag-Reducing Surface of a Real Shark Skin. *J. Hydrodyn.* **2011**, *23*, 204–211. [[CrossRef](#)]
98. Luo, Y.; Liu, Y.; Zhang, D.; NG, E.Y.K. Influence of morphology for drag reduction effect of sharkskin surface. *J. Mech. Med. Biol.* **2014**, *14*, 1450029. [[CrossRef](#)]
99. Luo, Y.; Yuan, L.; Li, J.; Wang, J. Boundary layer drag reduction research hypotheses derived from bio-inspired surface and recent advanced applications. *Micron* **2015**, *79*, 59–73. [[CrossRef](#)] [[PubMed](#)]

100. Martin, S.; Bhushan, B. Modeling and optimization of shark-inspired riblet geometries for low drag applications. *J. Colloid Interface Sci.* **2016**, *474*, 206–215. [[CrossRef](#)] [[PubMed](#)]
101. Fu, Y.F.; Yuan, C.Q.; Bai, X.Q. Marine drag reduction of shark skin inspired riblet surfaces. *Biosurface Biotribol.* **2017**, *3*, 11–24. [[CrossRef](#)]
102. Belhadjamor, M.; Belghith, S.; Mezlini, S.; El Mansori, M. Effect of the surface texturing scale on the self-clean function: Correlation between mechanical response and wetting behavior. *Tribol. Int.* **2017**, *111*, 91–99. [[CrossRef](#)]
103. Brajdic-Mitidieri, P.; Gosman, A.D.; Ioannides, E.; Spikes, H.A. CFD Analysis of a Low Friction Pocketed Pad Bearing. *J. Tribol.* **2005**, *127*, 803. [[CrossRef](#)]
104. Vakilian, M.; Gandjalikhan Nassab, S.A.; Kheirandish, Z. CFD-Based Thermohydrodynamic Analysis of Rayleigh Step Bearings Considering an Inertia Effect. *Tribol. Trans.* **2014**, *57*, 123–133. [[CrossRef](#)]
105. Ai, X.; Cheng, H.S.; Zheng, L. A Transient Model for Micro-Elastohydrodynamic Lubrication With Three-Dimensional Irregularities. *J. Tribol.* **1993**, *115*, 102. [[CrossRef](#)]
106. Chang, L.; Cusano, C.; Conry, T.F. Effects of Lubricant Rheology and Kinematic Conditions on Micro-Elastohydrodynamic Lubrication. *J. Tribol.* **1989**, *111*, 344. [[CrossRef](#)]
107. Chang, L.; Webster, M.N.; Jackson, A. A Line-Contact Micro-EHL Model With Three-Dimensional Surface Topography. *J. Tribol.* **1994**, *116*, 21. [[CrossRef](#)]
108. Kweh, C.C.; Evans, H.P.; Snidle, R.W. Micro-Elastohydrodynamic Lubrication of an Elliptical Contact With Transverse and Three-Dimensional Sinusoidal Roughness. *J. Tribol.* **1989**, *111*, 577. [[CrossRef](#)]
109. Lubrecht, A.A.; Ten Napel, W.E.; Bosma, R. The Influence of Longitudinal and Transverse Roughness on the Elastohydrodynamic Lubrication of Circular Contacts. *J. Tribol.* **1988**, *110*, 421. [[CrossRef](#)]
110. Kweh, C.C.; Patching, M.J.; Evans, H.P.; Snidle, R.W. Simulation of Elastohydrodynamic Contacts Between Rough Surfaces. *J. Tribol.* **1992**, *114*, 412. [[CrossRef](#)]
111. Venner, C.H.; ten Napel, W.E. Surface Roughness Effects in an EHL Line Contact. *J. Tribol.* **1992**, *114*, 616. [[CrossRef](#)]
112. Zhu, D.; Ai, X. Point Contact EHL Based on Optically Measured Three-Dimensional Rough Surfaces. *J. Tribol.* **1997**, *119*, 375. [[CrossRef](#)]
113. Xu, G.; Sadeghi, F. Thermal EHL Analysis of Circular Contacts With Measured Surface Roughness. *J. Tribol.* **1996**, *118*, 473. [[CrossRef](#)]
114. Hu, Y.-Z.; Zhu, D. A Full Numerical Solution to the Mixed Lubrication in Point Contacts. *J. Tribol.* **2000**, *122*, 1. [[CrossRef](#)]
115. Zhu, D.; Hu, Y.-Z. A Computer Program Package for the Prediction of EHL and Mixed Lubrication Characteristics, Friction, Subsurface Stresses and Flash Temperatures Based on Measured 3-D Surface Roughness. *Tribol. Trans.* **2001**, *44*, 383–390. [[CrossRef](#)]
116. Zhu, D.; Jane Wang, Q. Effect of Roughness Orientation on the Elastohydrodynamic Lubrication Film Thickness. *J. Tribol.* **2013**, *135*, 031501. [[CrossRef](#)]
117. Wang, X.; Liu, Y.; Zhu, D. Numerical Solution of Mixed Thermal Elastohydrodynamic Lubrication in Point Contacts With Three-Dimensional Surface Roughness. *J. Tribol.* **2016**, *139*, 011501. [[CrossRef](#)]
118. Ren, N.; Nanbu, T.; Yasuda, Y.; Zhu, D.; Wang, Q. Micro Textures in Concentrated-Conformal-Contact Lubrication: Effect of Distribution Patterns. *Tribol. Lett.* **2007**, *28*, 275–285. [[CrossRef](#)]
119. Wang, Q.J.; Zhu, D.; Zhou, R.; Hashimoto, F. Investigating the Effect of Surface Finish on Mixed EHL in Rolling and Rolling-Sliding Contacts. *Tribol. Trans.* **2008**, *51*, 748–761. [[CrossRef](#)]
120. Zhu, D.; Hu, Y.-Z. Effects of Rough Surface Topography and Orientation on the Characteristics of EHD and Mixed Lubrication in Both Circular and Elliptical Contacts. *Tribol. Trans.* **2001**, *44*, 391–398. [[CrossRef](#)]
121. Wang, Q.J.; Zhu, D. Virtual Texturing: Modeling the Performance of Lubricated Contacts of Engineered Surfaces. *J. Tribol.* **2005**, *127*, 722. [[CrossRef](#)]
122. Liu, Y.; Wang, Q.J.; Wang, W.; Hu, Y.; Zhu, D. Effects of Differential Scheme and Mesh Density on EHL Film Thickness in Point Contacts. *J. Tribol.* **2006**, *128*, 641. [[CrossRef](#)]
123. Zhu, D. On some aspects of numerical solutions of thin-film and mixed elastohydrodynamic lubrication. *Proc. Inst. Mech. Eng. Part J J. Eng. Tribol.* **2007**, *221*, 561–579. [[CrossRef](#)]
124. Ren, N.; Zhu, D.; Chen, W.W.; Liu, Y.; Wang, Q.J. A Three-Dimensional Deterministic Model for Rough Surface Line-Contact EHL Problems. *J. Tribol.* **2008**, *131*, 011501. [[CrossRef](#)]

125. Zhu, D.; Jane Wang, Q. Elastohydrodynamic Lubrication: A Gateway to Interfacial Mechanics—Review and Prospect. *J. Tribol.* **2011**, *133*, 041001. [[CrossRef](#)]
126. Zhu, D.; Nanbu, T.; Ren, N.; Yasuda, Y.; Wang, Q.J. Model-based virtual surface texturing for concentrated conformal-contact lubrication. *Proc. Inst. Mech. Eng. Part J J. Eng. Tribol.* **2010**, *224*, 685–696. [[CrossRef](#)]
127. Demirci, I.; Mezghani, S.; Yousfi, M.; Zahouani, H.; Mansori, M. El The Scale Effect of Roughness on Hydrodynamic Contact Friction. *Tribol. Trans.* **2012**, *55*, 705–712. [[CrossRef](#)]
128. Mezghani, S.; Demirci, I.; Zahouani, H.; El Mansori, M. The effect of groove texture patterns on piston-ring pack friction. *Precis. Eng.* **2012**, *36*, 210–217. [[CrossRef](#)]
129. Demirci, I.; Mezghani, S.; Yousfi, M.; El Mansori, M. Multiscale Analysis of the Roughness Effect on Lubricated Rough Contact. *J. Tribol.* **2013**, *136*, 011501. [[CrossRef](#)]
130. Profito, F.J.; Tomanik, E.; Zachariadis, D.C. Effect of cylinder liner wear on the mixed lubrication regime of TLOCs. *Tribol. Int.* **2016**, *93*, 723–732. [[CrossRef](#)]
131. Li, Y. *Multiphase Oil Transport at Complex Micro Geometry*; Massachusetts Institute of Technology: Cambridge, MA, USA, 2011.
132. Li, Y.; Chen, H.; Tian, T. A Deterministic Model for Lubricant Transport within Complex Geometry under Sliding Contact and its Application in the Interaction between the Oil Control Ring and Rough Liner in Internal Combustion Engines. In *Proceedings of the SAE Technical Paper Series*; SAE International: Warrendale, PA, USA, 2010; Volume 1.
133. Chen, H. *Modeling the Lubrication of the Piston Ring Pack of Internal Combustion Engines Using Deterministic Method*; Massachusetts Institute of Technology: Cambridge, MA, USA, 2011.
134. Chen, H.; Li, Y.; Tian, T. A Novel Approach to Model the Lubrication and Friction between the Twin-Land Oil Control Ring and Liner with Consideration of Micro Structure of the Liner Surface Finish in Internal Combustion Engines. In *Proceedings of the SAE Technical Paper Series*; SAE International: Warrendale, PA, USA, 2010; Volume 1.
135. Liao, K.; Liu, Y.; Kim, D.; Urzua, P.; Tian, T. Practical challenges in determining piston ring friction. *Proc. Inst. Mech. Eng. Part J J. Eng. Tribol.* **2013**, *227*, 112–125. [[CrossRef](#)]
136. Tomanik, E.; El Mansori, M.; Souza, R.; Profito, F. Effect of waviness and roughness on cylinder liner friction. *Tribol. Int.* **2018**, *120*, 547–555. [[CrossRef](#)]
137. Biboulet, N.; Bouassida, H.; Lubrecht, A.A. Cross hatched texture influence on the load carrying capacity of oil control rings. *Tribol. Int.* **2015**, *82*, 12–19. [[CrossRef](#)]
138. Noutary, M.-P.; Biboulet, N.; Lubrecht, A.A. Dimple influence on load carrying capacity of parallel surfaces. *Tribol. Int.* **2018**. [[CrossRef](#)]
139. Noutary, M.-P.; Biboulet, N.; Lubrecht, A.A. A robust piston ring lubrication solver: Influence of liner groove shape, depth and density. *Tribol. Int.* **2016**, *100*, 35–40. [[CrossRef](#)]
140. Minet, C.; Brunetière, N.; Tournier, B. A Deterministic Mixed Lubrication Model for Mechanical Seals. *J. Tribol.* **2011**, *133*, 042203. [[CrossRef](#)]
141. Pavliotis, G.A.; Stuart, A.M. *Multiscale Methods: Averaging and Homogenization*; Texts Applied in Mathematics; Springer: New York, NY, USA, 2008; ISBN 9788578110796.
142. Cioranescu, D.; Donato, P. *An Introduction to Homogenization*; Oxford University Press: Oxford, UK, 1999.
143. Weinan, E. *Principles of Multiscale Modeling*; Cambridge University Press: Cambridge, UK, 2011; ISBN 9781107096547.
144. Horstemeyer, M.F. Multiscale Modeling: A Review. In *Practical Aspects of Computational Chemistry*; Springer: Dordrecht, The Netherlands, 2009; pp. 87–135. ISBN 9789048126866.
145. Vakis, A.I.; Yastrebov, V.A.; Scheibert, J.; Nicola, L.; Dini, D.; Minfray, C.; Almqvist, A.; Paggi, M.; Lee, S.; Limbert, G.; et al. Modeling and simulation in tribology across scales: An overview. *Tribol. Int.* **2018**, *125*, 169–199. [[CrossRef](#)]
146. Tzeng, S.T.; Saibel, E. Surface roughness effect on slider bearing lubrication. *ASLE Trans.* **1967**, *10*, 334–348. [[CrossRef](#)]
147. Christensen, H. Stochastic Models for Hydrodynamic Lubrication of Rough Surfaces. *Proc. Inst. Mech. Eng.* **1969**, *184*, 1013–1026. [[CrossRef](#)]
148. Christensen, H. Some aspects of the functional influence of surface roughness in lubrication. *Wear* **1971**, *17*, 149–162. [[CrossRef](#)]
149. Christensen, H. A Theory of Mixed Lubrication. *Proc. Inst. Mech. Eng.* **1972**, *186*, 421–430. [[CrossRef](#)]

150. Chow, L.S.H.; Cheng, H.S. The Effect of Surface Roughness on the Average Film Thickness Between Lubricated Rollers. *J. Lubr. Technol.* **1976**, *98*, 117. [[CrossRef](#)]
151. Patir, N.; Cheng, H.S. Application of Average Flow Model to Lubrication Between Rough Sliding Surfaces. *J. Lubr. Technol.* **1979**, *101*, 220. [[CrossRef](#)]
152. Patir, N.; Cheng, H.S. An Average Flow Model for Determining Effects of Three-Dimensional Roughness on Partial Hydrodynamic Lubrication. *J. Lubr. Technol.* **1978**, *100*, 12. [[CrossRef](#)]
153. Elrod, H.G. A General Theory for Laminar Lubrication With Reynolds Roughness. *J. Lubr. Technol.* **1979**, *101*, 8. [[CrossRef](#)]
154. Tripp, J.H. Surface Roughness Effects in Hydrodynamic Lubrication: The Flow Factor Method. *J. Lubr. Technol.* **1983**, *105*, 458. [[CrossRef](#)]
155. de Kraker, A.; van Ostayen, R.A.J.; Rixen, D.J. Development of a texture averaged Reynolds equation. *Tribol. Int.* **2010**, *43*, 2100–2109. [[CrossRef](#)]
156. de Kraker, A.; van Ostayen, R.A.J.; van Beek, A.; Rixen, D.J. A Multiscale Method Modeling Surface Texture Effects. *J. Tribol.* **2007**, *129*, 221. [[CrossRef](#)]
157. Jocsak, J.; Li, Y.; Tian, T.; Wong, V.W. Analyzing the Effects of Three-Dimensional Cylinder Liner Surface Texture on Ring-Pack Performance with a Focus on Honing Groove Cross-Hatch Angle. In Proceedings of the ASME 2005 Internal Combustion Engine Division Fall Technical Conference (ICEF2005), Ottawa, ON, Canada, 11–14 September 2005; pp. 621–632.
158. Leighton, M.; Rahmani, R.; Rahnejat, H. Surface-specific flow factors for prediction of friction of cross-hatched surfaces. *Surf. Topogr. Metrol. Prop.* **2016**, *4*, 025002. [[CrossRef](#)]
159. Bartel, D.; Bobach, L.; Illner, T.; Deters, L. Simulating transient wear characteristics of journal bearings subjected to mixed friction. *Proc. Inst. Mech. Eng. Part J J. Eng. Tribol.* **2012**, *226*, 1095–1108. [[CrossRef](#)]
160. Kim, T.W.; Cho, Y.J. The Flow Factors Considering the Elastic Deformation for the Rough Surface with a Non-Gaussian Height Distribution. *Tribol. Trans.* **2008**, *51*, 213–220. [[CrossRef](#)]
161. Peeken, H.J.; Knoll, G.; Rienäcker, A.; Lang, J.; Schönen, R. On the Numerical Determination of Flow Factors. *J. Tribol.* **1997**, *119*, 259. [[CrossRef](#)]
162. Pusterhofer, M.; Bergmann, P.; Summer, F.; Grün, F.; Brand, C. A Novel Approach for Modeling Surface Effects in Hydrodynamic Lubrication. *Lubricants* **2018**, *6*, 27. [[CrossRef](#)]
163. Dobrica, M.B.; Fillon, M.; Maspeyrot, P. Mixed Elastohydrodynamic Lubrication in a Partial Journal Bearing—Comparison Between Deterministic and Stochastic Models. *J. Tribol.* **2006**, *128*, 778. [[CrossRef](#)]
164. Bayada, G.; Chambat, M. New Models in the Theory of the Hydrodynamic Lubrication of Rough Surfaces. *J. Tribol.* **1988**, *110*, 402. [[CrossRef](#)]
165. Bayada, G.; Cid, B.; Vázquez, C. Two-scale homogenization study of a Reynolds-Rod elastohydrodynamic model. *Math. Model. Methods Appl. Sci.* **2003**, *13*, 259–293. [[CrossRef](#)]
166. Bayada, G.; Faure, J.B. A Double Scale Analysis Approach of the Reynolds Roughness Comments and Application to the Journal Bearing. *J. Tribol.* **1989**, *111*, 323. [[CrossRef](#)]
167. Bayada, G.; Martin, S.; Vázquez, C. Two-scale homogenization of a hydrodynamic Elrod–Adams model. *Asymptot. Anal.* **2005**, *44*, 75–110.
168. Bayada, G.; Martin, S.; Vázquez, C. An Average Flow Model of the Reynolds Roughness Including a Mass-Flow Preserving Cavitation Model. *J. Tribol.* **2005**, *127*, 793. [[CrossRef](#)]
169. Jai, M. Homogenization and two-scale convergence of the compressible Reynolds lubrication equation modelling the flying characteristics of a rough magnetic head over a rough rigid-disk surface. *ESAIM Math. Model. Numer. Anal.* **1995**, *29*, 199–233. [[CrossRef](#)]
170. Jai, M.; Bou-Saïd, B. A Comparison of Homogenization and Averaging Techniques for the Treatment of Roughness in Slip-Flow-Modified Reynolds Equation. *J. Tribol.* **2002**, *124*, 327. [[CrossRef](#)]
171. Kane, M.; Bou-Saïd, B. Comparison of Homogenization and Direct Techniques for the Treatment of Roughness in Incompressible Lubrication. *J. Tribol.* **2004**, *126*, 733. [[CrossRef](#)]
172. Buscaglia, G.C.; Jai, M. Homogenization of the Generalized Reynolds Equation for Ultra-Thin Gas Films and Its Resolution by FEM. *J. Tribol.* **2004**, *126*, 547. [[CrossRef](#)]
173. Buscaglia, G.; Ciuperca, I.; Jai, M. Homogenization of the transient Reynolds equation. *Asymptot. Anal.* **2002**, *32*, 131–152.
174. Buscaglia, G.C.; Jai, M. A new numerical scheme for non uniform homogenized problems: Application to the non linear Reynolds compressible equation. *Math. Probl. Eng.* **2001**, *7*, 355–378. [[CrossRef](#)]

175. Prat, M.; Plouraboué, F.; Letalleur, N. Averaged Reynolds equation for flows between rough surfaces in sliding motion. *Transp. Porous Media* **2002**, *48*, 291–313. [[CrossRef](#)]
176. Almqvist, A.; Dasht, J. The homogenization process of the Reynolds equation describing compressible liquid flow. *Tribol. Int.* **2006**, *39*, 994–1002. [[CrossRef](#)]
177. Almqvist, A.; Essel, E.K.; Fabricius, J.; Wall, P. Reiterated homogenization applied in hydrodynamic lubrication. *Proc. Inst. Mech. Eng. Part J J. Eng. Tribol.* **2008**, *222*, 827–841. [[CrossRef](#)]
178. Almqvist, A.; Essel, E.K.; Persson, L.-E.; Wall, P. Homogenization of the unstationary incompressible Reynolds equation. *Tribol. Int.* **2007**, *40*, 1344–1350. [[CrossRef](#)]
179. Almqvist, A. Homogenization of the Reynolds Equation Governing Hydrodynamic Flow in a Rotating Device. *J. Tribol.* **2011**, *133*, 021705. [[CrossRef](#)]
180. Almqvist, A.; Fabricius, J.; Spencer, A.; Wall, P. Similarities and Differences Between the Flow Factor Method by Patir and Cheng and Homogenization. *J. Tribol.* **2011**, *133*, 031702. [[CrossRef](#)]
181. Almqvist, A.; Lukkassen, D.; Meidell, A.; Wall, P. New concepts of homogenization applied in rough surface hydrodynamic lubrication. *Int. J. Eng. Sci.* **2007**, *45*, 139–154. [[CrossRef](#)]
182. Spencer, A.; Almqvist, A.; Larsson, R. A semi-deterministic texture-roughness model of the piston ring–cylinder liner contact. *Proc. Inst. Mech. Eng. Part J J. Eng. Tribol.* **2011**, *225*, 325–333. [[CrossRef](#)]
183. Söderfjäll, M.; Almqvist, A.; Larsson, R. A model for twin land oil control rings. *Tribol. Int.* **2016**, *95*, 475–482. [[CrossRef](#)]
184. Sahlin, F.; Larsson, R.; Almqvist, A.; Lugt, P.M.; Marklund, P. A mixed lubrication model incorporating measured surface topography. Part 1: Theory of flow factors. *Proc. Inst. Mech. Eng. Part J J. Eng. Tribol.* **2010**, *224*, 335–351. [[CrossRef](#)]
185. Sahlin, F.; Larsson, R.; Marklund, P.; Almqvist, A.; Lugt, P.M. A mixed lubrication model incorporating measured surface topography. Part 2: Roughness treatment, model validation, and simulation. *Proc. Inst. Mech. Eng. Part J J. Eng. Tribol.* **2010**, *224*, 353–365. [[CrossRef](#)]
186. Hu, Y.; Meng, X.; Xie, Y. A computationally efficient mass-conservation-based, two-scale approach to modeling cylinder liner topography changes during running-in. *Wear* **2017**, *386*, 139–156. [[CrossRef](#)]
187. Hu, Y.; Meng, X.; Xie, Y. A new efficient flow continuity lubrication model for the piston ring-pack with consideration of oil storage of the cross-hatched texture. *Tribol. Int.* **2018**, *119*, 443–463. [[CrossRef](#)]
188. Rom, M.; Muller, S. A Reduced Basis Method for the Homogenized Reynolds Equation Applied to Textured Surfaces. *Commun. Comput. Phys.* **2018**, *24*, 481–509. [[CrossRef](#)]
189. Scaraggi, M.; Carbone, G.; Dini, D. Lubrication in soft rough contacts: A novel homogenized approach. Part II—Discussion. *Soft Matter* **2011**, *7*, 10407. [[CrossRef](#)]
190. Scaraggi, M.; Carbone, G.; Persson, B.N.J.; Dini, D. Lubrication in soft rough contacts: A novel homogenized approach. Part I—Theory. *Soft Matter* **2011**, *7*, 10395. [[CrossRef](#)]
191. Scaraggi, M. Optimal Textures for Increasing the Load Support in a Thrust Bearing Pad Geometry. *Tribol. Lett.* **2014**, *53*, 127–143. [[CrossRef](#)]
192. Scaraggi, M. Textured surface hydrodynamic lubrication: Discussion. *Tribol. Lett.* **2012**, *48*, 375–391. [[CrossRef](#)]
193. Scaraggi, M. Lubrication of textured surfaces: A general theory for flow and shear stress factors. *Phys. Rev. E* **2012**, *86*, 026314. [[CrossRef](#)]
194. Gao, L.; Hewson, R. A Multiscale Framework for EHL and Micro-EHL. *Tribol. Trans.* **2012**, *55*, 713–722. [[CrossRef](#)]
195. Gao, L.; de Boer, G.; Hewson, R. The role of micro-cavitation on EHL: A study using a multiscale mass conserving approach. *Tribol. Int.* **2015**, *90*, 324–331. [[CrossRef](#)]
196. Lahmar, M.; Bou-Saïd, B.; Tichy, J. The homogenization method of roughness analysis in turbulent lubrication. *Proc. Inst. Mech. Eng. Part J J. Eng. Tribol.* **2013**, *227*, 1090–1100. [[CrossRef](#)]
197. Waseem, A.; Temizer, İ.; Kato, J.; Terada, K. Homogenization-based design of surface textures in hydrodynamic lubrication. *Int. J. Numer. Methods Eng.* **2016**, *108*, 1427–1450. [[CrossRef](#)]
198. Waseem, A.; Temizer, İ.; Kato, J.; Terada, K. Micro-texture design and optimization in hydrodynamic lubrication via two-scale analysis. *Struct. Multidiscip. Optim.* **2017**, *56*, 227–248. [[CrossRef](#)]
199. Yildiran, I.N.; Temizer, I.; Çetin, B. Homogenization in Hydrodynamic Lubrication: Microscopic Regimes and Re-Entrant Textures. *J. Tribol.* **2017**, *140*, 011701. [[CrossRef](#)]

200. Gu, C.; Meng, X.; Xie, Y.; Zhang, D. Mixed lubrication problems in the presence of textures: An efficient solution to the cavitation problem with consideration of roughness effects. *Tribol. Int.* **2016**, *103*, 516–528. [[CrossRef](#)]
201. Ma, C.; Duan, Y.; Yu, B.; Sun, J.; Tu, Q. The comprehensive effect of surface texture and roughness under hydrodynamic and mixed lubrication conditions. *Proc. Inst. Mech. Eng. Part J J. Eng. Tribol.* **2017**, *231*, 1307–1319. [[CrossRef](#)]
202. Xie, Y.; Li, Y.; Suo, S.; Liu, X.; Li, J.; Wang, Y. A mass-conservative average flow model based on finite element method for complex textured surfaces. *Sci. China Physics Mech. Astron.* **2013**, *56*, 1909–1919. [[CrossRef](#)]
203. Profito, F.J.; Vladescu, S.-C.; Reddyhoff, T.; Dini, D. Experimental Validation of a Mixed-Lubrication Regime Model for Textured Piston-Ring-Liner Contacts. *Mater. Perform. Charact.* **2017**, *6*, 112–129. [[CrossRef](#)]
204. Zhang, H.; Hua, M.; Dong, G.; Zhang, D.; Chin, K.-S. A mixed lubrication model for studying tribological behaviors of surface texturing. *Tribol. Int.* **2016**, *93*, 583–592. [[CrossRef](#)]
205. Meng, X.; Gu, C.; Xie, Y. Elasto-plastic contact of rough surfaces: A mixed-lubrication model for the textured surface analysis. *Meccanica* **2017**, *52*, 1541–1559. [[CrossRef](#)]
206. Qiu, Y.; Khonsari, M.M. Performance Analysis of Full-Film Textured Surfaces With Consideration of Roughness Effects. *J. Tribol.* **2011**, *133*, 021704. [[CrossRef](#)]
207. Brunetière, N.; Tournier, B. Numerical analysis of a surface-textured mechanical seal operating in mixed lubrication regime. *Tribol. Int.* **2012**, *49*, 80–89. [[CrossRef](#)]
208. Venner, C.H.; Lubrecht, A.A. (Eds.) *Multi-Level Methods in Lubrication*; Elsevier: Amsterdam, The Netherlands, 2000.
209. Zhao, J.; Vollebregt, E.A.H.; Oosterlee, C.W. A full multigrid method for linear complementary problems arising from elastic normal contact problems. *Math. Model. Anal.* **2014**, *19*, 216–240. [[CrossRef](#)]
210. Zhang, B.; Boffy, H.; Venner, C.H. Multigrid solution of 2D and 3D stress fields in contact mechanics of anisotropic inhomogeneous materials. *Tribol. Int.* **2019**. [[CrossRef](#)]
211. Checo, H.M.; Jai, M.; Buscaglia, G.C. An Improved Fixed-Point Algorithm to Solve the Lubrication Problem with Cavitation. *Mecánica Comput.* **2016**, *34*, 1973–1987.
212. Boffy, H.; Venner, C.H. Multigrid solution of the 3D stress field in strongly heterogeneous materials. *Tribol. Int.* **2014**, *74*, 121–129. [[CrossRef](#)]
213. Goodyer, C.E.; Berzins, M. Parallelization and scalability issues of a multilevel elasto-hydrodynamic lubrication solver. *Concurr. Comput. Pract. Exp.* **2007**, *19*, 369–396. [[CrossRef](#)]
214. Li, L.; Bogy, D.B. A Local Adaptive Multigrid Control Volume Method for the Air Bearing Problem in Hard Disk Drives. *J. Tribol.* **2013**, *135*, 032001. [[CrossRef](#)]
215. Lu, H.; Berzins, M.; Goodyer, C.E.; Jimack, P.K.; Walkley, M. Adaptive high-order finite element solution of transient elasto-hydrodynamic lubrication problems. *Proc. Inst. Mech. Eng. Part J J. Eng. Tribol.* **2006**, *220*, 215–225. [[CrossRef](#)]
216. Nilsson, B.; Hansbo, P. Adaptive finite element methods for hydrodynamic lubrication with cavitation. *Int. J. Numer. Methods Eng.* **2007**, *72*, 1584–1604. [[CrossRef](#)]
217. Lu, H.; Berzins, M.; Goodyer, C.E.; Jimack, P.K. Adaptive high-order Discontinuous Galerkin solution of elasto-hydrodynamic lubrication point contact problems. *Adv. Eng. Softw.* **2012**, *45*, 313–324. [[CrossRef](#)]
218. Ahmed, S.; Goodyer, C.E.; Jimack, P.K. An adaptive finite element procedure for fully-coupled point contact elasto-hydrodynamic lubrication problems. *Comput. Methods Appl. Mech. Eng.* **2014**, *282*, 1–21. [[CrossRef](#)]
219. Babuška, I.; Osborn, J.E. Generalized Finite Element Methods: Their Performance and Their Relation to Mixed Methods. *SIAM J. Numer. Anal.* **1983**, *20*, 510–536. [[CrossRef](#)]
220. Efendiev, Y.; Hou, T. *Multiscale Finite Element Methods*; Springer: New York, NY, USA, 2009; ISBN 978-0-387-09495-3.
221. Moyner, O.; Lie, K.-A. The Multiscale Finite Volume Method on Unstructured Grids. In Proceedings of the SPE Reservoir Simulation Symposium, The Woodlands, TX, USA, 18–20 February 2013; Society of Petroleum Engineers: Richardson, TX, USA, 2013.
222. Jiang, L.; Mishev, I.D. Mixed Multiscale Finite Volume Methods for Elliptic Problems in Two-Phase Flow Simulations. *Commun. Comput. Phys.* **2012**, *11*, 19–47. [[CrossRef](#)]
223. Jenny, P.; Lee, S.; Tchelepi, H. Multi-scale finite-volume method for elliptic problems in subsurface flow simulation. *J. Comput. Phys.* **2003**, *187*, 47–67. [[CrossRef](#)]

224. Weinan, E.; Engquist, B.; Li, X.; Ren, W.; Vanden-Eijnden, E. Heterogeneous Multiscale Methods: A Review. *Commun. Comput. Phys.* **2007**, *2*, 367–450.
225. Steinhauser, M.O. *Computational Multiscale Modeling of Fluids and Solids*; Springer: Berlin/Heidelberg, Germany, 2017; ISBN 978-3-662-53222-5.
226. Pei, S.; Ma, S.; Xu, H.; Wang, F.; Zhang, Y. A multiscale method of modeling surface texture in hydrodynamic regime. *Tribol. Int.* **2011**, *44*, 1810–1818. [[CrossRef](#)]
227. Pei, S.; Xu, H.; Shi, F. A deterministic multiscale computation method for rough surface lubrication. *Tribol. Int.* **2016**, *94*, 502–508. [[CrossRef](#)]
228. Pei, S.; Xu, H.; Yun, M.; Shi, F.; Hong, J. Effects of surface texture on the lubrication performance of the floating ring bearing. *Tribol. Int.* **2016**, *102*, 143–153. [[CrossRef](#)]
229. Nyemeck, A.P.; Brunetière, N.; Tournier, B. A Multiscale Approach to the Mixed Lubrication Regime: Application to Mechanical Seals. *Tribol. Lett.* **2012**, *47*, 417–429. [[CrossRef](#)]
230. Nyemeck, A.P.; Brunetiere, N.; Tournier, B. A Mixed Thermoelastohydrodynamic Lubrication Analysis of Mechanical Face Seals by a Multiscale Approach. *Tribol. Trans.* **2015**, *58*, 836–848. [[CrossRef](#)]
231. Pérez-Ràfols, F.; Larsson, R.; Lundström, S.; Wall, P.; Almqvist, A. A stochastic two-scale model for pressure-driven flow between rough surfaces. *Proc. R. Soc. A Math. Phys. Eng. Sci.* **2016**, *472*, 20160069. [[CrossRef](#)] [[PubMed](#)]
232. De Boer, G.N.; Hewson, R.W.; Thompson, H.M.; Gao, L.; Toropov, V.V. Two-scale EHL: Three-dimensional topography in tilted-pad bearings. *Tribol. Int.* **2014**, *79*, 111–125. [[CrossRef](#)]
233. Brunetière, N.; Francisco, A. Multiscale Modeling Applied to the Hydrodynamic Lubrication of Rough Surfaces for Computation Time Reduction. *Lubricants* **2018**, *6*, 83. [[CrossRef](#)]
234. Costagliola, G.; Bosia, F.; Pugno, N.M. Hierarchical Spring-Block Model for Multiscale Friction Problems. *ACS Biomater. Sci. Eng.* **2017**, *3*, 2845–2852. [[CrossRef](#)]
235. Costagliola, G.; Bosia, F.; Pugno, N.M. A 2-D model for friction of complex anisotropic surfaces. *J. Mech. Phys. Solids* **2018**, *112*, 50–65. [[CrossRef](#)]
236. Costagliola, G.; Bosia, F.; Pugno, N.M. Static and dynamic friction of hierarchical surfaces. *Phys. Rev. E* **2016**, *94*, 063003. [[CrossRef](#)]
237. Costagliola, G.; Bosia, F.; Pugno, N.M. Tuning friction with composite hierarchical surfaces. *Tribol. Int.* **2017**, *115*, 261–267. [[CrossRef](#)]
238. Wu, X.; Ge, Z.; Niu, H.; Ruan, J.; Zhang, J. Edge effect factor affecting the tribological properties in water of protrusion surface textures on stainless steel. *Biosurface Biotribol.* **2018**, *4*, 46–49. [[CrossRef](#)]
239. Joshi, G.S.; Putignano, C.; Gaudioso, C.; Stark, T.; Kiedrowski, T.; Ancona, A.; Carbone, G. Effects of the micro surface texturing in lubricated non-conformal point contacts. *Tribol. Int.* **2018**, *127*, 296–301. [[CrossRef](#)]
240. Wang, X.; Wang, J.; Zhang, B.; Huang, W. Design principles for the area density of dimple patterns. *Proc. Inst. Mech. Eng. Part J J. Eng. Tribol.* **2014**, *229*, 538–546. [[CrossRef](#)]
241. Greiner, C.; Merz, T.; Braun, D.; Codrignani, A.; Magagnato, F. Optimum dimple diameter for friction reduction with laser surface texturing: The effect of velocity gradient. *Surf. Topogr. Metrol. Prop.* **2015**, *3*, 044001. [[CrossRef](#)]
242. Sahlin, F.; Glavatskih, S.B.; Almqvist, T.; Larsson, R. Two-Dimensional CFD-Analysis of Micro-Patterned Surfaces in Hydrodynamic Lubrication. *J. Tribol.* **2005**, *127*, 96. [[CrossRef](#)]

